α2δ-1 switches the phenotype of synaptic AMPA receptors by physically disrupting heteromeric subunit assembly

Lingyong Li[1,2,5], **Shao-Rui Chen**[1,5], **Meng-Hua Zhou**[1], **Li Wang**[1], **De-Pei Li**[1,3], **Hong Chen**[1], **Garam Lee**[4], **Vasanthi Jayaraman**[4], **Hui-Lin Pan**[1,6,*]

[1]Center for Neuroscience and Pain Research, Department of Anesthesiology and Perioperative Medicine, University of Texas MD Anderson Cancer Center, Houston, TX 77030, USA

[2]Department of Neuroscience, Baylor College of Medicine, Houston, TX 77030, USA

[3]Department of Medicine, University of Missouri School of Medicine, Columbia, MO 65211, USA

[4]Department of Biochemistry and Molecular Biology, University of Texas Health Science Center, Houston, TX 77030, USA

[5]These authors contributed equally

[6]Lead contact

SUMMARY

Many neurological disorders show an increased prevalence of GluA2-lacking, Ca^{2+}-permeable AMPA receptors (CP-AMPARs), which dramatically alters synaptic function. However, the molecular mechanism underlying this distinct synaptic plasticity remains enigmatic. Here, we show that nerve injury potentiates postsynaptic, but not presynaptic, CP-AMPARs in the spinal dorsal horn via α2δ-1. Overexpressing α2δ-1, previously regarded as a Ca^{2+} channel subunit, augments CP-AMPAR levels at the cell surface and synapse. Mechanistically, α2δ-1 physically interacts with both GluA1 and GluA2 via its C terminus, inhibits the GluA1/GluA2 heteromeric assembly, and increases GluA2 retention in the endoplasmic reticulum. Consequently, α2δ-1 diminishes the availability and synaptic expression of GluA1/GluA2 heterotetramers in the spinal cord in neuropathic pain. Inhibiting α2δ-1 with gabapentin or disrupting the α2δ-1-AMPAR complex fully restores the intracellular assembly and synaptic dominance of heteromeric GluA1/GluA2 receptors. Thus, α2δ-1 is a pivotal AMPAR-interacting protein that controls the subunit composition and Ca^{2+} permeability of postsynaptic AMPARs.

Graphical abstract

In brief

Li et al. show that α2δ-1 directly interacts with GluA1 and GluA2 subunits via its C terminus and disrupts intracellular assembly of GluA1/GluA2 heteromers. Gabapentinoids reduce neuropathic pain by restoring assembly and synaptic prevalence of heteromeric AMPA receptors in the spinal cord.

INTRODUCTION

AMPA-type glutamate receptors (AMPARs) are the predominant postsynaptic receptors involved in fast excitatory neurotransmission in the central nervous system. Among the four pore-forming AMPAR subunits (GluA1–GluA4), GluA2 is a key determinant of the biophysical properties of AMPARs and is subject to unique Q/R editing (Greger et al., 2003; Sommer et al., 1991). Most mature GluA2 proteins contain an arginine residue (R) in the M2 re-entrant loop at position 607 in place of the genomically encoded glutamine (Q607). The added positive charge to the pore region by R607 prevents both passage of Ca^{2+} and block by intracellular polyamines, as well as decreasing single-channel conductance. Thus, GluA2-containing AMPARs are impermeable to Ca^{2+} (CI-AMPARs), whereas GluA2-lacking AMPARs are permeable to Ca^{2+} (CP-AMPARs) and show unique inward rectification at positive holding potentials (Isaac et al., 2007; Traynelis et al., 2010). Most AMPARs in the adult brain and spinal cord consist of heteromeric GluA1/GluA2

subunits, which render AMPARs Ca^{2+} impermeable (Isaac et al., 2007). This impermeability is essential to maintain an appropriately low cytoplasmic Ca^{2+} level under physiological conditions. Changes in the composition of AMPAR subunits are associated with many forms of synaptic plasticity, and the switch from GluA2-containing CI-AMPARs to GluA2-lacking CP-AMPARs at synapses occurs in many neurological disorders (Henley and Wilkinson, 2016). In particular, the increased prevalence of postsynaptic CP-AMPARs in the spinal dorsal horn contributes to the development of chronic neuropathic pain (Chen et al., 2013a, 2019a), which remains refractory to current treatment. Despite the recognition of the significance of CP-AMPARs, the mechanism responsible for this distinct switch in the synaptic AMPAR phenotype in pathological conditions remains enigmatic.

Neuropathic pain is associated with upregulation of α2δ-1 in the dorsal root ganglion and spinal cord (Luo et al., 2002), and α2δ-1 is the main target of gabapentinoids used clinically for treating neuropathic pain. Recent studies indicate that α2δ-1 directly interacts with NMDA-type glutamate receptors (NMDARs) to promote their synaptic delivery in neuropathic pain, independent of voltage-gated Ca^{2+} channels (Chen et al., 2018, 2019b). Intriguingly, an AMPAR antagonist and gabapentin produce a synergistic effect on neuropathic pain (Chen et al., 2000), also suggesting a potential link between α2δ-1 and AMPARs. We thus conducted a series of *in vitro* and *in vivo* studies to explore the association of α2δ-1 with CP-AMPARs. Here we report another previously unrecognized function of α2δ-1, which prevents heteromeric assembly of GluA1/GluA2 subunits and their synaptic expression by physically interacting with both GluA1 and GluA2. Inhibiting α2δ-1 or uncoupling the α2δ-1-AMPAR interaction restores intracellular assembly and synaptic incorporation of heteromeric AMPARs in neuropathic pain. Therefore, α2δ-1 promotes synaptic dominance of CP-AMPARs by directly regulating their subunit composition. Our findings not only advance mechanistic understanding of synaptic AMPAR plasticity but also have important therapeutic implications for treating neuropathic pain and other neurological disorders.

RESULTS

α2δ-1 is essential for the dominance of synaptic CP-AMPARs in the spinal cord in neuropathic pain

To determine the relationship between increased α2δ-1 expression and CP-AMPARs in neuropathic pain, we first determined whether overexpression of α2δ-1 (encoded by *Cacna2d1*) at the spinal cord level increases postsynaptic CP-AMPAR activity in spinal dorsal horn neurons. We intrathecally injected α2δ-1-expressing lentiviral vectors, which effectively induce transgene expression in the spinal cord (Li et al., 2016) and cause long-lasting pain hypersensitivity (Chen et al., 2018). Pain hypersensitivity induced by α2δ-1 overexpression was readily reversed by intrathecal injection of IEM-1460, a selective CP-AMPAR open-channel blocker (Chen et al., 2013a; Sebe et al., 2017; Twomey et al., 2018) (n = 9 rats; Figure 1A). IEM-1460 had no effect on baseline withdrawal thresholds in rats treated with a control vector (n = 8 rats; Figure 1A).

CP-AMPARs exhibit characteristic inward rectification at positive holding potentials (Bowie and Mayer, 1995; Isaac et al., 2007). Thus, to determine the relationship between α2δ-1

and synaptic CP-AMPAR levels, we assessed the current-voltage (I-V) relationship of AMPAR-mediated excitatory postsynaptic currents (AMPAR-EPSCs) of spinal lamina II neurons elicited by stimulation of the dorsal root (Chen et al., 2013a, 2019a) in rats injected with vectors expressing *Cacna2d1* (encoding α2δ-1) or control vectors. In dorsal horn neurons of control-vector-injected rats, I-V plots showed a near-linear relationship of AMPAR-EPSCs (n = 11 neurons; Figures 1B-1D), indicating that synaptic AMPAR-EPSCs are mediated mainly by GluA2-containing CI-AMPARs. In contrast, in rats injected with *Cacna2d1*-expressing vectors, I-V plots of AMPAR-EPSCs of dorsal horn neurons showed inward rectification at positive holding potentials and a reduced rectification index (n = 15 neurons; Figures 1B-1D). These data indicate that increased α2δ-1 expression potentiates synaptic CP-AMPAR activity in the spinal cord, which contributes to the development of neuropathic pain.

We next used *Cacna2d1* knockout (KO) mice to study the role of α2δ-1 in synaptic CP-AMPARs in the spinal cord potentiated by nerve injury. Similar to what we reported previously in nerve-injured rats (Chen et al., 2013a), I-V plots of AMPAR-EPSCs showed inward rectification in spinal lamina II neurons of wild-type (WT) mice subjected to spared nerve injury (SNI) (n = 15 neurons; Figures 1E-1G). Remarkably, in lamina II neurons in *Cacna2d1* KO mice subjected to SNI, we observed a near-linear I-V relationship of AMPAR-EPSCs (n = 13 neurons; Figures 1E-1G). These findings demonstrate that α2δ-1 is critically involved in nerve-injury-induced potentiation of postsynaptic CP-AMPARs in the spinal cord.

We also determined whether nerve injury increases presynaptic CP-AMPARs in the spinal cord. Blocking postsynaptic CP-AMPARs via intracellular dialysis of IEM-1460 for 15 min significantly reduced the amplitude of evoked EPSCs in lamina II neurons in SNI-treated WT mice (n = 13 neurons), but not in sham control WT mice (n = 14 neurons). In contrast, intracellular dialysis of IEM-1460 had no effect on evoked EPSCs in SNI-treated α2δ-1 KO mice (n = 15 neurons; Figure S1). These results further indicate that nerve injury potentiates postsynaptic CP-AMPARs in the spinal cord through α2δ-1. However, when postsynaptic CP-AMPARs were blocked by IEM-1460, subsequent bath application of IEM-1460 had no effect on the amplitude of evoked EPSCs in all 3 groups of mice (Figure S1). These data suggest that nerve injury does not induce functional CP-AMPARs at primary afferent central terminals.

α2δ-1 preferentially alters the I-V relationship and Ca^{2+} permeability of heteromeric GluA1/GluA2 receptors

To determine whether α2δ-1 regulates the phenotype of homomeric and heteromeric AMPARs independent of other AMPAR-interacting proteins in neurons, we determined the effect of α2δ-1 on the I-V relationship of AMPAR currents reconstituted using heterologous expression in HEK293 cells. Because the heteromeric GluA1/GluA2 subunits are the predominant AMPARs mediating fast excitatory synaptic transmission in the CNS (Traynelis et al., 2010; Wenthold et al., 1996), we examined the effect of α2δ-1 on homomeric GluA1 and GluA2 and heteromeric GluA1/GluA2 receptors. Whole-cell recordings of HEK293 cells transfected with one AMPAR subunit showed characteristic I-V

relationships of glutamate-elicited currents reconstituted with homomeric GluA1, GluA2, or GluA2(Q607) receptors, as reported previously (Burnashev et al., 1992) (Figures S2A and S2B). Coexpression of α2δ-1 had no effect on the I-V relationship or rectification indexes of AMPAR currents in cells expressing homomeric GluA1, GluA2, or GluA2(Q607) (Figures S2A and S2B).

Transfection of both GluA1 and GluA2 in cell lines produces predominant expression of heteromeric over homomeric AMPARs, suggesting that heteromeric assembly of GluA1/GluA2 is strongly favored over homomeric assemblies (Lu et al., 2009; Rossmann et al., 2011). In contrast to edited GluA2, unedited GluA2(Q607) readily forms homomers and traffics through the endoplasmic reticulum (ER) to the plasma membrane (Greger et al., 2003; Henley and Wilkinson, 2016). In HEK293 cells transfected with GluA1/GluA2, but not in those cells transfected with GluA1/GluA2(Q607), we found a linear I-V relationship of glutamate-elicited currents (Figures S2C and S2D). Coexpression with α2δ-1, but not α2δ-2 or α2δ-3, in HEK293 cells transfected with GluA1/GluA2 changed the I-V relationship from linear to inwardly rectifying (Figures S2C and S2D). There was no significant difference in the current density of GluA1/GluA2 receptors between cells with α2δ-1 and cells without α2δ-1 (260.79 ± 35.27 versus 238.14 ± 33.59 pA/pF; n = 16 cells/group). Coexpression of α2δ-1 had no effect on the I-V relationship of AMPAR currents reconstituted with GluA1 and GluA2(Q607) (Figures S2C and S2D).

To determine whether the α2δ-1-induced inward rectification of GluA1/GluA2 receptor currents was associated with an increase in Ca^{2+} permeability (P_{Ca}/P_{Na}), we compared the reversal potential of glutamate-evoked currents in solutions containing 1 mM Ca^{2+} (low Ca^{2+}) or 30 mM Ca^{2+} (high Ca^{2+}) (Soto et al., 2007). Switching from low Ca^{2+} to high Ca^{2+} caused a greater shift in the reversal potentials of heteromeric GluA1/GluA2 currents toward negative values in cells without α2δ-1 than in cells with α2δ-1 (Figures S2E and S2F). From the shift in reversal potentials, we calculated P_{Ca}/P_{Na}, which showed a large increase from 0.26 ± 0.01 in cells without α2δ-1 (n = 11 cells) to 0.54 ± 0.06 in cells with α2δ-1 (n = 12 cells), suggesting that α2δ-1 coexpression increases the Ca^{2+} permeability of GluA1/GluA2 receptors. These *in vitro* data indicate that α2δ-1 promotes GluA2-lacking CP-AMPARs on plasma membranes by directly regulating the composition and/or surface expression of GluA1 and GluA2 subunits.

α2δ-1, but not α2δ-2 or α2δ-3, physically interacts with GluA1 and GluA2

The functional significance of α2δ-1 in regulating the subunit composition of AMPARs prompted us to examine whether α2δ-1 directly interacts with AMPARs. To determine the interaction between α2δ-1 and AMPARs *in vitro*, we performed coimmunoprecipitation (coIP) using protein extracts from HEK293 cells expressing green fluorescent protein (GFP)-tagged α2δ-1, together with FLAG-tagged stargazin, GluA1, GluA2, or GluA1/GluA2. We used stargazin (γ2), a protein that interacts with AMPARs (Tomita et al., 2005), as a control. Both GluA1 and GluA2, but not stargazin, were precipitated by an anti-GFP antibody (Figure 2A). In contrast, neither GluA1 nor GluA2 was coprecipitated with α2δ-2 or α2δ-3 (Figure S2G). We also performed reverse coIP using HEK293 cells transfected with α2δ-1 and GluA1-GFP, GluA2-GFP, GluA1-GFP/GluA2, or GluA2-GFP/

GluA1. Again, an anti-GFP antibody consistently precipitated α2δ-1 proteins (Figures 2B and 2C), suggesting that α2δ-1 interacts with GluA1 and GluA2 directly.

We then used luminescence resonance energy transfer (LRET) to assess the α2δ-1 interaction with GluA1 or GluA2 on the plasma membrane of live HEK293 cells. LRET between terbium-labeled GluA1 homomeric receptors and yellow fluorescent protein (YFP)-tagged α2δ-1 yielded a single exponential decay (Figures S3A and S3B), and this lifetime, along with the donor-only lifetime (Figure S3B), provided a distance of 51.21 ± 0.15 Å between YFP on the N terminus of α2δ-1 and terbium on the N terminus of GluA1.

Similar measurements of terbium-labeled GluA2 homomeric receptors and YFP-α2δ-1 yielded a single exponential decay (Figures S3C and S3D; Table S1) with a corresponding distance of 54.35 ± 0.41 Å between YFP on the N terminus of α2δ-1 and terbium on the N terminus of GluA2. Based on these distances and the constraint placing the membrane-spanning segments together, an LRET nano-positioning model is shown between a GluA2 homomeric receptor and α2δ-1 (Figure S3G), which suggests that the two proteins interact closely. Given the high sequence homology between GluA2 and GluA1 and the similar LRET-based distances with respect to α2δ-1, we conclude that there is also close interaction between α2δ-1 and GluA1 homomeric proteins and that the C terminus of α2δ-1 may interact with the transmembrane domain of GluA1 and GluA2 (Figure S3G).

To determine whether α2δ-1 coexpression affects surface expression of heteromeric GluA1/GluA2 receptors, we labeled GFP on the N terminus of GluA1 and terbium on the N terminus of GluA2. Under these conditions, only the heteromeric receptors had donor and acceptor fluorophores, so the LRET signal was specific to the heteromeric GluA1/GluA2 receptors. The LRET lifetimes of heteromeric GluA1/GluA2 receptors corresponded to a distance of 54.63 ± 0.50 Å in the absence of α2δ-1 (Figure S3E; Table S1). However, coexpression with α2δ-1 markedly reduced the initial fluorescence intensity (Figure S3F). Because the initial intensity provided an estimate of the number of receptors on the cell surface, this reduction suggests a 10-fold decrease in the number of heteromeric GluA1/GluA2 receptors in the presence of α2δ-1. Given the extremely small intensity of the heteromeric receptors on the surface, it was difficult to reliably determine the lifetimes of heteromeric GluA1/GluA2 receptors in the presence of α2δ-1.

To determine the interaction between α2δ-1 and AMPARs *in vivo*, we conducted coIP using protein extracts from dorsal spinal cords of rats. GluA1 and GluA2 were precipitated by an anti-α2δ-1 antibody, but not by an irrelevant immunoglobulin G (IgG) (Figure 2D). In addition, using protein extracts from the spinal cord tissues of human donors, we demonstrated that α2δ-1 coimmunoprecipitated with both GluA1 and GluA2 (Figure 2E), indicating that this crosstalk is conserved across species. Altogether, these results indicate that α2δ-1 physically interacts with GluA1 and GluA2 subunits *in vitro* and *in vivo*.

The C terminus of α2δ-1 is required for its interaction with AMPARs

We next attempted to identify the molecular determinants of α2δ-1 involved in its interaction with AMPARs. The large α2 protein is entirely extracellular, whereas the small δ protein has a transmembrane C-terminal domain. We previously showed that α2δ-1 directly

interacts with NMDARs via its C terminus (Chen et al., 2018). Here, we coexpressed six α2δ-1 constructs—full-length α2δ-1, von Willebrand factor type A (VWA) domain, α2, δ-1, δ-1 without the C terminus (δ-1 CT), and the C terminus of δ-1, each with a C-terminal protein C (PC) tag for purification—with GluA1/GluA2 subunits in HEK293 cells. PC tag affinity purification revealed that GluA1 and GluA2 copurified with full-length α2δ-1, δ-1, and the C terminus, but not with VWA, α2, or δ-1 CT (Figure 2F). Thus, α2δ-1 interacts with GluA1 and GluA2 predominantly through its C-terminal domain.

To confirm that the C terminus of α2δ-1 is required for its interaction with AMPARs, we designed a 30-amino-acid peptide (VSGLNPSLWSIFGLQFILLWLVSGSRHYLW) mimicking the C terminus of α2δ-1 to determine whether the peptide would uncouple the α2δ-1-AMPAR interaction. We fused the C terminus-mimicking peptide to a cell-penetrating peptide, Tat (YGRKKRRQRRR), to produce an α2δ-1CT-Tat peptide to target intracellular α2δ-1-AMPAR complexes (Chen et al., 2018). In HEK293 cells cotransfected with FLAG-α2δ-1 and GluA1/GluA2, treatment with α2δ-1CT-Tat peptide (1 μM for 30 min), but not a Tat-fused scrambled control peptide, caused a large reduction in the protein amount of GluA1 and GluA2 coprecipitated by an anti-FLAG antibody (Figure 2G). These data support the predominant role of the C terminus of α2δ-1 in its interaction with AMPARs.

The C terminus of α2δ-1 is critically involved in neuropathic pain and in the dominance of synaptic CP-AMPARs in spinal cords

Treatment with α2δ-1Tat peptide effectively attenuates neuropathic pain in animal models (Chen et al., 2018, 2019b). To determine whether expressing the C terminus of α2δ-1 reverses nerve-injury-induced chronic pain, we tested the effect of lentiviral vector-mediated expression of the C-terminal sequence of α2δ-1 on pain hypersensitivity in rats 2 weeks after spinal nerve ligation (SNL). In SNL rats, intrathecal injection of a lentiviral vector encoding the C-terminal peptide sequence of α2δ-1 (n = 8 rats), but not a control vector (n = 7 rats), gradually and fully reversed the reduced mechanical and thermal withdrawal thresholds within 3 weeks after vector treatment (Figure 3A). However, in sham control rats, treatment with either the vector expressing the α2δ-1 C terminus or the control vector had no effect on the withdrawal thresholds (Figure 3A).

We also determined the functional significance of the C-terminal domain of α2δ-1 in α2δ-1-induced chronic pain. In *Cacna2d1* KO mice, we intrathecally injected lentiviral vectors expressing WT α2δ-1 or an α2δ-1 chimera in which the C terminus of α2δ-1 was replaced with that of α2δ-3 (α2δ-1$_{CT(α2δ-3)}$), as described previously (Chen et al., 2018). Re-expression of WT α2δ-1 in *Cacna2d1* KO mice markedly reduced the mechanical and thermal withdrawal thresholds (n = 10 mice; Figure 3B). In contrast, intrathecal injection of lentiviral vectors expressing α2δ-1$_{CT(α2δ-3)}$ had no effect on the withdrawal thresholds of *Cacna2d1* KO mice (n = 10 mice; Figure 3B). Strikingly, re-expression of WT α2δ-1 (n = 15 neurons), but not α2δ-1$_{CT(α2δ-3)}$ (n = 16 neurons), in *Cacna2d1* KO mice recapitulated nerve-injury-induced inward rectification of AMPAR-EPSCs in spinal dorsal horn neurons (Figures 3C-3E). Furthermore, bath application of IEM-1460 (100 μM) for 6 min normalized the reduced rectification index of AMPAR-EPSCs of lamina II neurons

in *Cacna2d1* KO mice injected with WT α2δ-1 vectors (Figures 3C-3E). These results indicate that the C terminus of α2δ-1 is required for α2δ-1-mediated synaptic expression of CP-AMPARs in the spinal cord in neuropathic pain.

α2δ-1 diminishes surface and synaptic expression of GluA2 and heteromeric GluA1/GluA2 receptors

We next determined whether interaction with α2δ-1 differentially controls protein levels of GluA1 and GluA2 subunits on the cell surface. HEK293 cells were cotransfected with GluA1/GluA2 and α2δ-1, α2δ-2, or α2δ-3, and cell surface proteins were isolated using biotin labeling (Chen et al., 2018). Coexpression of α2δ-1, but not α2δ-2 or α2δ-3, markedly reduced the amount of GluA2 surface proteins (Figure 4A). However, coexpression of α2δ-1, α2δ-2, or α2δ-3 had no effect on the surface protein level of GluA1 (Figure 4A). Furthermore, we conducted coIP using protein extracts from plasma membranes of HEK293 cells transfected with GluA1/GluA2-GFP or GluA2/GluA1-GFP with or without α2δ-1. CoIP with an anti-GFP antibody consistently showed that α2δ-1 coexpression diminished the amount of heteromeric GluA1/GluA2 complexes on the plasma membrane (Figure 4B).

To determine whether nerve injury differentially affects synaptic expression of GluA1 and GluA2 in spinal cords, we isolated synaptosomes from the dorsal spinal cords of rats 3 weeks after they were subjected to SNL or sham surgery. The protein level of GluA2, but not GluA1, in spinal cord synaptosomes was lower in SNL rats than in sham control rats (Figure 4C). In addition, coIP showed that SNL markedly reduced the protein levels of heteromeric GluA1/GluA2 and GluA2-α2δ-1 complexes but increased the protein level of GluA1-α2δ-1 complexes in spinal cord synaptosomes (Figures 4D and 4E). Thus, α2δ-1 coexpression and nerve injury diminish GluA2 and heteromeric GluA1/GluA2 receptors on the cell surface and at the spinal cord synapse.

α2δ-1 coupling prevents heteromeric assembly of GluA1/GluA2 and increases retention of GluA2 in the ER

In neuropathic pain, the dominance of synaptic CP-AMPARs is associated with reduced GluA2 levels on synaptic membranes and increased GluA2 levels in cytoplasmic fractions (Chen et al., 2013a, 2019a), raising the possibility of altered intracellular AMPAR assembly. Functional AMPARs are tetrameric complexes assembled from four homomeric or heteromeric combinations of subunits as a dimer of dimers (Mayer, 2006). In the absence of GluA2, GluA1 assembles into homomeric tetramers that can be rapidly exported from the ER and trafficked to the plasma membrane (Greger et al., 2002, 2003). In the presence of the edited GluA2(R607), GluA1 prefers to assemble with GluA2 into GluA1/GluA2 heterotetramers, which follow the GluA1 trafficking rule and override ER retention of GluA2, whereas GluA2 is generally unassembled and retained within the ER (Greger et al., 2002). Because the synaptic expression of AMPARs depends on the availability of assembled AMPAR subunits, we determined whether α2δ-1 controls the heteromeric assembly of GluA1 and GluA2 in the ER.

To this end, we used an ER isolation kit to obtain ER-enriched fractions from HEK293 cells transfected with GluA1-GFP/GluA2 or GluA2-GFP/GluA1 with or without α2δ-1. Immunoblotting showed that coexpression with α2δ-1 markedly increased the protein amount of GluA2, but not GluA1, in ER-enriched fractions (Figures 5A and 5B). In addition, coIP revealed that coexpression with α2δ-1 caused a large reduction in the protein level of heteromeric GluA1/GluA2 in the ER (Figures 5A and 5B).

We next determined the protein levels of GluA1 and GluA2 in ER-enriched fractions from spinal cords of rats subjected to SNL. As expected, immunoblotting and coIP showed that SNL significantly increased protein levels of GluA2 and α2δ-1 but diminished protein levels of heteromeric GluA1/GluA2 in ER-enriched fractions, compared with levels in sham controls (Figures 5C-5E). Furthermore, the amount of GluA1-α2δ-1 and GluA2-α2δ-1 protein complexes in the ER fraction was higher in SNL rats than in sham controls (Figures 5D and 5E).

To determine whether α2δ-1 overexpression alters heteromeric GluA1/GluA2 receptors in the ER of spinal cords, we intrathecally injected lentiviral vectors expressing α2δ-1 in rats. Three weeks after vector injection, ER-enriched fractions were isolated from the dorsal spinal cords. Immunoblotting showed that overexpression of α2δ-1 substantially increased the amount of GluA2 proteins in the spinal ER fractions (Figures S4A and S4B). In addition, coIP showed that the protein level of heteromeric GluA1/GluA2 in the spinal ER fractions was lower in rats treated with α2δ-1-expressing lentiviral vectors than in rats treated with control vectors (Figures S4C and S4D). These data indicate that α2δ-1 disrupts heteromeric assembly of GluA2-containing CI-AMPARs and increases the retention of GluA2 in the ER.

We then used Duolink proximity ligation assay (PLA) as a complementary approach to assess the effect of α2δ-1 on the proximity of GluA1 and GluA2 *in situ*. HEK293 cells were cotransfected with GluA1/GluA2 and α2δ-1-IRES-GFP or GFP alone. The PLA signal of GluA1/GluA2 protein complexes was detected using mouse anti-GluA1 and rabbit anti-GluA2 antibodies. In cells transfected with GluA1/GluA2 without α2δ-1, the GluA1/GluA2 interaction signal was clearly visible on plasma membranes and in intracellular compartments (Figure 5F). In contrast, cotransfection with α2δ-1 diminished the GluA1/GluA2 interaction signal in HEK293 cells (Figure 5F).

In addition, we performed PLA using spinal cord sections from SNL and sham control rats. The GluA1/GluA2 interaction signals were readily detected in the spinal dorsal horn of sham control rats (Figure 5G). In contrast, the GluA1/GluA2 interaction signal was markedly reduced in the superficial dorsal horn of SNL rats (Figure 5G), which is consistent with the distribution of α2δ-1 in the spinal dorsal horn (Cole et al., 2005). These results are compatible with the interpretation that α2δ-1, via direct interaction with GluA1 and GluA2, prevents the heteromeric assembly of GluA1/GluA2 receptors *in vitro* and *in vivo*.

Gabapentin and the α2δ-1 C terminus peptide restore heteromeric assembly and surface expression of GluA1/GluA2 receptors diminished by α2δ-1 coexpression

Recent studies show that gabapentinoids reduce neuropathic pain primarily by targeting α2δ-1-bound NMDARs (Chen et al., 2018, 2019b; Huang et al., 2020). Because of the

importance of α2δ-1 in regulating the subunit composition of CP-AMPARs, we reasoned that gabapentin might diminish synaptic CP-AMPARs as an additional mechanism of its therapeutic effects on neuropathic pain. We thus determined the effects of inhibiting α2δ-1 with gabapentin or disrupting the α2δ-1-AMPAR interaction with α2δ-1CT-Tat peptide on CP-AMPARs caused by α2δ-1 coexpression.

To directly determine the effects of gabapentin and α2δ-1CT-Tat peptide on α2δ-1-coexpression-induced Ca^{2+} permeability of AMPARs, we conducted Ca^{2+} imaging in live HEK293 cells cotransfected with GluA1/GluA2 and GCaMP, a genetically encoded calcium indicator (Chen et al., 2013b). Bath application of 5 mM glutamate only slightly increased the GCaMP fluorescence signal in cells transfected with GluA1/GluA2 alone. In contrast, glutamate application caused a large increase in the GCaMP signal in cells coexpressing GluA1/GluA2 and α2δ-1 (Figures 6A-6C). At the end of the imaging experiments, bath application of a Ca^{2+} ionophore, ionomycin (1 μM), markedly increased the GCaMP signal in both groups of HEK293 cells (Figures 6A and 6B). Pretreatment of HEK293 cells with 100 μM gabapentin or 1 μM α2δ-1CT-Tat peptide, but not 1 μM Tat-fused control peptide, diminished the glutamate-elicited GCaMP signal in cells cotransfected with GluA1/GluA2 and α2δ-1 (Figure 6C).

We next used PLA to assess the effect of gabapentin or α2δ-1CT-Tat peptide on the heteromeric assembly of GluA1/GluA2 in HEK293 cells cotransfected with α2δ-1-IRES-GFP or α2δ-1R217A-IRES-GFP (α2δ-1R217 is the binding site of gabapentinoids) (Field et al., 2006). Treatment with gabapentin or α2δ-1CT-Tat peptide, but not control peptide, restored the GluA1/GluA2 interaction signal diminished in cells coexpressing GluA1/GluA2 and α2δ-1 (Figure 6D). However, gabapentin did not rescue the GluA1/GluA2 interaction signal that was diminished by coexpression with α2δ-1R217A mutant in HEK293 cells (Figure 6E).

We also determined the effect of gabapentin and α2δ-1CT-Tat peptide on the I-V relationship of glutamate-elicited currents in HEK293 cells expressing GluA1/GluA2/α2δ-1 or GluA1/GluA2/α2δ-1R217A mutant. Treatment with 100 μM gabapentin restored the linear I-V relationship of glutamate-elicited currents in cells expressing GluA1/GluA2/α2δ-1 (n = 12 cells; Figures 6F and 6G). Furthermore, treatment with 1 μM α2δ-1CT-Tat peptide, but not 1 μM control peptide, changed the I-V relationship of GluA1/GluA2 currents from inwardly rectifying to linear (n = 12 cells/group; Figures 6F and 6G). However, in HEK293 cells cotransfected with GluA1/GluA2 and α2δ-1R217A mutant, gabapentin failed to restore the reduced rectification index of glutamate-elicited currents (n = 11 cells; Figures 6F and 6G).

To determine whether gabapentin reverses α2δ-1-induced reduction in cell surface expression of GluA2, we used biotinylation to label and isolate the cell-surface proteins from HEK293 cells coexpressing heteromeric GluA1/GluA2 with α2δ-1 or α2δ-1R217A mutant. Coexpression with α2δ-1 or α2δ-1R217A mutant markedly decreased the protein level of GluA2, but not GluA1, on the membrane surface (Figure S5A). Treatment with gabapentin normalized the surface protein level of GluA2 that had been reduced by α2δ-1 coexpression. However, in cells whose GluA2 surface protein levels were diminished by

α2δ-1R217A coexpression, gabapentin had no effect on these levels (Figure S5A). In addition, treatment with α2δ-1CT-Tat peptide normalized the surface protein level of GluA2 that had been decreased by α2δ-1 coexpression in HEK293 cells (Figure S5B).

Furthermore, to determine the effect of gabapentin and α2δ-1CT-Tat peptide on the heteromeric assembly of GluA1/GluA2 in the ER and their surface expression, we transfected HEK293 cells with α2δ-1 and GluA1-GFP/GluA2 or GluA2-GFP/GluA1 and then treated cells with gabapentin or α2δ-1CT-Tat peptide. We conducted coIP using an anti-GFP antibody with ER-enriched fractions and cell surface protein extracts. Coexpression with α2δ-1 markedly reduced the protein levels of heteromeric GluA1/GluA2 in the ER and plasma membrane fractions (Figures S6 and S7). Remarkably, treatment with gabapentin or α2δ-1CT-Tat peptide normalized the α2δ-1-induced reduction in the amount of heteromeric GluA1/GluA2 receptors in the ER and on the cell surface (Figures S6 and S7). Gabapentin treatment had no effect on the amount of protein complexes formed by α2δ-1-GluA1 or α2δ-1-GluA2 in cells coexpressing FLAG-α2δ-1 and GluA1 or GluA2 (Figure S8). Collectively, these *in vitro* data provide substantial evidence that inhibiting α2δ-1 or disrupting the α2δ-1-AMPAR coupling rescues the heteromeric assembly of GluA1/GluA2 receptors in the ER and their cell surface expression from diminishment by α2δ-1.

Gabapentin and the α2δ-1CT-Tat peptide restore postsynaptic expression of GluA2-containing AMPARs in the spinal cord diminished in neuropathic pain

To determine whether gabapentin or α2δ-1CT-Tat peptide reverses nerve-injury-induced reduction in synaptic expression and heteromeric assembly of GluA1/GluA2 in the spinal cord, we treated dorsal spinal cord slices from SNL rats with vehicle, gabapentin, control peptide, or α2δ-1CT-Tat peptide for 30 min and then isolated the synaptosomes and ER-enriched fractions from the tissue slices. Immunoblotting showed that gabapentin or α2δ-1CT-Tat peptide reversed the decreased protein level of GluA2 in the spinal synaptosomes from SNL rats (Figure 7A). In addition, treatment with gabapentin or α2δ-1CT-Tat peptide normalized the increased level of GluA2 in the ER-enriched fractions from dorsal spinal cords of SNL rats (Figure 7B). However, treatment with either gabapentin or α2δ-1CT-Tat peptide had no effect on the protein level of GluA2 in spinal cord synaptosomes or ER-enriched fractions obtained from sham control rats (Figures 7A and 7B). Furthermore, coIP using spinal cord synaptosomes showed that gabapentin or α2δ-1CT-Tat peptide fully restored the protein level of heteromeric GluA1/GluA2 that was diminished by SNL (Figure 7C). These results indicate that gabapentin and α2δ-1CT-Tat peptide separately are capable of reversing GluA2 redistribution in the synapse and ER and the reduction in synaptic expression of heteromeric GluA1/GluA2 receptors in the spinal cord induced by nerve injury.

In addition, we determined the effects of gabapentin and α2δ-1CT-Tat peptide on the synaptic prevalence of CP-AMPARs in the spinal dorsal horn in neuropathic pain. The spinal cord slices were obtained from SNL rats 2–3 weeks after surgery and were treated with gabapentin (100 μM), α2δ-1CT-Tat peptide (1 μM), or control peptide (1 μM) for 30 min. The I-V plots of AMPAR-EPSCs in spinal dorsal horn neurons showed a linear relationship

after treatment with gabapentin (n = 12 neurons) or α2δ-1CT-Tat peptide (n = 13 neurons; Figures 7D and 7E). In contrast, the I-V relationship of AMPAR-EPSCs still exhibited characteristic inward rectification in dorsal horn neurons of SNL spinal cord slices treated with vehicle (n = 10 neurons) or control peptide (n = 15 neurons; Figures 7D and 7E).

α2δ-1 is also upregulated in the spinal cord of diabetic rats (Luo et al., 2002), and gabapentinoids are effective in reducing neuropathic pain in patients with diabetes (Rosenstock et al., 2004). Diabetic neuropathic pain is associated with increased CP-AMPARs, but not increased NMDAR activity, in spinal cord synapses (Chen et al., 2019a). We therefore determined the effect of gabapentin and α2δ-1CT-Tat peptide on synaptic CP-AMPARs in a rat model of diabetic neuropathic pain. As expected, treatment of spinal cord slices of diabetic rats with gabapentin (n = 17 neurons) or α2δ-1CT-Tat peptide (n = 16 neurons) changed the I-V relationship of AMPAR-EPSCs from inwardly rectifying to linear in dorsal horn neurons (Figures 7F and 7G). Therefore, inhibiting α2δ-1 or disrupting the α2δ-1-AMPAR interaction restores the dominance of postsynaptic GluA2-containing AMPARs that have been diminished in neuropathic pain conditions.

DISCUSSION

Our study provides substantial evidence that α2δ-1 is a crucial regulator of AMPARs and promotes postsynaptic dominance of CP-AMPARs. Prolonged synaptic incorporation of CP-AMPARs can result in excessive Ca^{2+} influx, leading to neuronal dysfunction and damage. In previous studies (Chen et al., 2013a, 2019a), the switch to synaptic CP-AMPARs in neuropathic pain was assumed to result from GluA2 internalization in the spinal cord. However, this cannot explain diminution of intracellular GluA1/GluA2 heteromers. We discovered in this study that the predominant role of α2δ-1 in regulating AMPARs is its ability to directly interact with GluA1 and GluA2 to disrupt their heteromeric assembly. α2δ-1 can switch the composition of synaptic AMPAR subunits by interfering with the intracellular assembly of GluA2-containing AMPARs.

The convergent evidence from our study supports the following holistic view about the role of α2δ-1 in the phenotype switch of synaptic AMPARs: Under normal conditions, the α2δ-1 protein level is low in the ER, and α2δ-1-free GluA1 and GluA2 preferentially and efficiently form heteromers. The assembled GluA1/GluA2 heterotetramers can be rapidly exported from the ER and trafficked to the cell surface and synapse (Gregeret al., 2003; Henley and Wilkinson, 2016). In neuropathic pain, however, α2δ-1 is upregulated and forms protein complexes with GluA1 and GluA2, preventing their heteromeric assembly in the ER of the spinal dorsal horn. But coupling to α2δ-1 does not affect the assembly of GluA1 homotetramers, which continue to traffic to the synapse. The inability of GluA2 to assemble with GluA1 to form heterotetramers in the presence of α2δ-1 leads to subcellular redistribution of GluA2: accumulation in the ER and reduction on the synapse. Because AMPARs are highly dynamic and undergo constitutive trafficking to and from the cell surface, the diminished amount of GluA2-containing CI-AMPARs at synapses likely results from the reduced availability of assembled GluA2-containing receptors in the ER. As a result, GluA2-containing heteromers at spinal cord synapses are largely replaced by homomeric GluA1 receptors (CP-AMPARs) in neuropathic pain.

Our findings indicate that α2δ-1 has a pivotal role in activity-dependent glutamatergic synaptic plasticity. At the spinal cord level, both potentiated NMDAR activity and increased prevalence of CP-AMPARs are involved in the development of neuropathic pain (Chen et al., 2013a, 2014; Zhou et al., 2012). By increasing NMDAR trafficking and promoting CP-AMPARs at spinal cord synapses, α2δ-1 not only strengthens glutamatergic transmission but also impairs normal synaptic inhibition by γ-aminobutyric acid (GABA) and glycine, thus sustaining chronic neuropathic pain through Ca^{2+}-dependent signaling, such as calpain-mediated KCC2 proteolysis (Li et al., 2016; Zhou et al., 2012). Several AMPAR-interacting proteins also mediate the trafficking and/or distribution of AMPARs. Among them, protein interacting with C kinase-1 (PICK1) mediates the clustering of AMPARs at the membrane surface, and glutamate receptor-interacting protein (GRIP) is involved in the stabilization of intracellular AMPARs (Xia et al., 1999). In addition, transmembrane AMPAR regulatory proteins (TARPs), including γ2, γ7, and γ8, which were originally considered Ca^{2+} channel subunits, can directly interact with AMPARs to regulate their localization and channel characteristics (Studniarczyk et al., 2013; Tomita et al., 2005). α2δ-1 likely interferes with the heteromeric assembly of AMPARs independent of other AMPAR-interacting proteins present in neurons, because the actions of α2δ-1 on AMPARs were recapitulated using a heterologous expression system in our study.

We demonstrated that the C terminus of α2δ-1 is essential for α2δ-1-mediated CP-AMPARs in spinal cord synapses and for the development of chronic pain. In contrast to the full-length α2δ-1 protein, α2δ-1 CT peptide does not have α2 protein, which is highly glycosylated (Tétreault et al., 2016) and is required for full-length α2δ-1-mediated trafficking and interference of GluA1/A2 heteromeric assembly. α2δ-1 CT peptide, via competitive binding to GluA1/GluA2, minimizes the interaction of full-length α2δ-1 with AMPARs to restore the postsynaptic dominance of GluA2-containing CI-AMPAR in neuropathic pain. Although the C terminus is required for α2δ-1's physical interaction with AMPARs, the heteromeric assembly of GluA1 and GluA2 occurs mainly via their N-terminal domain (NTD) and ligand binding domain (LBD) and the GluA1 signal peptide (He et al., 2016; Rossmann et al., 2011). It is unclear exactly how α2δ-1 interferes with the spatial assembly of GluA1/GluA2 heteromers in the ER. In addition, α2δ-1 is highly expressed in many brain regions and is expected to similarly regulate AMPAR subunit composition. CP-AMPARs are involved in the pathogenesis of Alzheimer disease (Whitehead et al., 2017), Parkinson disease (Kobylecki et al., 2010), epilepsy (Friedman and Koudinov, 1999), drug addiction (Conrad et al., 2008), chronic stress (Kuniishi et al., 2020), neurogenic hypertension (Li et al., 2012), and ischemic stroke (Noh et al., 2005). Given the well-recognized role of CP-AMPARs in these neurological disorders, it is crucial to determine to what extent α2δ-1 mediates the increased synaptic CP-AMPARs under these conditions so that rational treatments can be designed.

Our findings also advance our understanding of the molecular mechanism responsible for the therapeutic effect of gabapentinoids on neuropathic pain. Gabapentin has no effect on Ca^{2+} channel activity (Chen et al., 2018; Rock et al., 1993) or α2δ-1-thrombospondin interaction (El-Awaad et al., 2019). In this study, we showed that although gabapentin does not affect α2δ-1's interaction with homomeric GluA1 or GluA2, it inhibits α2δ-1's function to prevent heteromeric assembly of GluA1/GluA2 receptors. It is uncertain how

gabapentin impedes α2δ-1's ability to disrupt the heteromeric assembly of AMPARs. Because gabapentinoids bind to the α2 protein (near its N terminus) (Field et al., 2006), which is close to the NTD/LBD of GluA1/GluA2, gabapentin may inhibit the spatial assembly of GluA1/GluA2 heterotetramers by altering the conformation of α2δ-1 proteins and thereby interfering with the NTD/LBD of GluA1/GluA2. In addition, gabapentin may inhibit trafficking of α2δ-1-bound GluA1 homomers. Through these two actions, gabapentin could restore the assembly and postsynaptic dominance of GluA1/GluA2 heteromers in the spinal cord in neuropathic pain. In traumatic nerve-injury-induced chronic pain, the *in vivo* actions of α2δ-1CT peptide and gabapentinoids likely involve inhibition of both α2δ-1-bound NMDARs and CP-AMPARs. However, chemotherapy-induced chronic pain is caused mainly by α2δ-1-mediated presynaptic NMDARs (Chen et al., 2019b), whereas diabetic neuropathic pain is associated with increased activity of CP-AMPARs, but not NMDARs, in the spinal cord (Chen et al., 2019a). Thus, the analgesic effects of α2δ-1CT peptide and gabapentinoids are likely by targeting α2δ-1-bound NMDARs in chemotherapy-induced neuropathic pain and by inhibiting CP-AMPARs in diabetic neuropathic pain.

In conclusion, our study reveals that α2δ-1 switches the phenotype of postsynaptic AMPARs by disrupting heteromeric receptor tetramerization. Because of its dual role in concurrently potentiating the number of NMDARs and CP-AMPARs at synapses, α2δ-1 has remarkable abilities in elevating intracellular Ca^{2+} levels and in augmenting excitatory synaptic activity. Thus, α2δ-1 likely serves as a master regulator to orchestrate both NMDAR- and AMPAR-mediated synaptic plasticity in neuropathic pain. The action of α2δ-1 can be recapitulated *in vitro*, suggesting that the role of α2δ-1 in regulating NMDARs and AMPARs is not limited to the spinal cord. On this basis, gabapentinoids and drugs acting on the α2δ-1 C terminus may restore normal synaptic function in neuropathic pain and other neurological disorders by targeting α2δ-1-bound NMDARs and CP-AMPARs.

STAR★METHODS

RESOURCE AVAILABILITY

Lead contact—Further information and requests for resources and reagents should be directed to and will be fulfilled by the Lead Contact, Hui-Lin Pan (huilinpan@mdanderson.org)

Materials availability—The materials generated in this study are available upon reasonable request to the Lead Contact.

Data and code availability—This study did not generate any unique datasets or code.

EXPERIMENTAL MODELS AND SUBJECT DETAILS

Rats—Male Sprague-Dawley rats (9–11 weeks of age, Harlan, Indianapolis, IN) were used in this study. We used L5 and L6 spinal nerve ligation (SNL) as an experimental model of neuropathic pain as previously described (Chen et al., 2000). Control rats underwent a sham surgical procedure without nerve ligation. For diabetic induction, rats were given a

single intraperitoneal injection of streptozotocin (STZ; 60 mg/kg; Sigma-Aldrich, St. Louis, MO) freshly dissolved in 0.9% sterile saline (Chen et al., 2019a). Diabetes was confirmed by measuring the blood glucose concentration using ACCU-CHEK test strips 2 weeks after STZ administration. Neuropathic pain in diabetic rats was confirmed by examining nociceptive thresholds using an Ugo Basile analgesiometer (Varese, Italy), as described previously (Chen et al., 2019a). The procedures and experimental protocols were approved by the Animal Care and Use Committee (approval #1186-RN02) of The University of Texas MD Anderson Cancer Center and conformed to the National Institutes of Health guidelines for the ethical use of animals.

Mice—Conventional *Cacna2d1* knockout mice (C57BL/6 genetic background) were generated as described previously (Fuller-Bicer et al., 2009). Two breeding pairs of *Cacna2d1*$^{+/-}$ mice were originally obtained from Medical Research Council (Harwell Didcot, Oxfordshire, UK), and *Cacna2d1*$^{-/-}$ mice and *Cacna2d1*$^{+/+}$ (wild-type) littermates were obtained by breeding the heterozygous mice and confirmed by PCR genotyping. For neuropathic pain induction, spared nerve injury (SNI) was performed on both male and female mice (10–11 weeks of age) under 2% isoflurane-induced anesthesia, as described previously (Chen et al., 2018). We ligated and sectioned the left common peroneal and tibial nerves, leaving the sural nerve intact. The sham procedure consisted of the same surgery without nerve ligation and sectioning. All the experiments were approved by Animal Care and Use Committee (approval #1174-RN02) and conducted at The University of Texas MD Anderson Cancer Center.

HEK293 and HEK293FT Cell Lines—HEK293 and HEK293FT cells were maintained in Dulbecco's modified Eagle's medium supplemented with 10% FBS and 1% penicillin/streptomycin in a humidified incubator at 37°C and 5% CO_2.

Human Spinal Cord Tissues—Frozen human lumbar spinal cord tissues from 4 human donors (2 men and 2 women; age range, 18–42 years; postmortem interval, 17–29 h) were acquired from the University of Maryland Brain and Tissue Bank, an NIH-funded NeuroBioBank Repository.

METHOD DETAILS

Behavioral Assessments of Nociception—To detect tactile allodynia, we applied a series of calibrated von Frey filaments (Stoelting, Wood Dale, IL) perpendicular to the plantar surface of the hindpaw with sufficient force to bend the filament for 6 s. Brisk withdrawal or paw flinching was considered to be a positive response. If there was no response, the filament of the next greater force was applied. After a response, the filament of the next lower force was applied. We calculated the tactile stimulus force that produced a 50% likelihood of a withdrawal response using the "up-down" method (Chaplan et al., 1994; Chen et al., 2000). Thermal nociception was measured using a radiant heat stimulus by placing rats on the glass surface maintained constantly at 30°C (IITC Life Science). To quantify mechanical nociception, we conducted the paw pressure test on the hindpaw by using a Ugo Basile analgesiometer. To activate the device, a foot pedal was pressed, triggering a motor that applied a constantly increasing force on a linear scale. When

the animal displayed pain by either withdrawing its paw or vocalizing, the pedal was immediately released, and the animal's nociceptive threshold was read on the scale (Chen et al., 2018). Investigators performing the behavioral tests were blinded to the treatments.

DNA Constructs and Lentiviral Vector Preparation—The rat cDNAs of GluA1, GluA2, and α2δ-1 (encoded by *Cacna2d1*) were all expressed in the expression vector pcDNA 3.1. The GFP-tagged GluA1 (C terminus), GFP-tagged GluA2 (C terminus), α2δ-2 (encoded by *Cacna2d2*), α2δ-3 (encoded by *Cacna2d3*), and HA-tagged α2δ-1, HA-tagged α2δ-2, and HA-tagged α2δ-3 constructs were obtained from Addgene (Watertown, MA). Flag-tagged stargazin was gifted from Dr. V Jayaraman's laboratory. To generate N-terminal tagged fusion constructs (Flag-α2δ-1 and GFP-α2δ-1), the coding sequences of Flag and GFP were inserted after the predicted signal peptide cleavage site of α2δ-1 by using recombinant PCR techniques. The mutant α2δ-1R217A was generated by mutating the gabapentin binding site on α2δ-1 (the R217A mutant, also termed R241A when amino acid numbering included the N-terminal signal peptide sequence of α2δ-1) (Chen et al., 2018). The protein C (PC)-tagged α2δ-1, α2, δ-1, and von Willebrand factor type A (VWA) constructs were kindly provided by Dr. C. Eroglu (Duke University, Durham, NC). The C terminus of α2δ-1 (residues 1059-1091) was deleted from δ-1-PC to generate δ-1 CT-PC. The C terminus of α2δ-1 (residues 1059-1091) was fused with the PC tag to generate a CT-PC construct. The amino acid numbering includes the N-terminal signal sequence of α2δ-1. The constructs were made using the QuikChange Site-Directed Mutagenesis Kit (Agilent Technologies, Santa Clara, CA) or In-Fusion HD Cloning Plus (Takara Bio USA, Inc., Mountain View, CA). All cDNA clones and mutated constructs were confirmed by DNA sequencing.

The full-length coding sequence of enhanced green fluorescent protein (GFP), rat α2δ-1 tagged with GFP at the N terminus, or rat α2δ-1 tagged with GFP at the C terminus (residues 1059-1091) was cloned into the lentiviral vector pLenti6/V5-DEST. The virus was produced using the ViraPower system (Invitrogen, Carlsbad, CA) as described by the manufacturer. Briefly, the vectors were transfected into HEK293FT cells using Lipofectamine 3000. The virus-containing supernatant was collected 72 h after transfection and filtered through 0.45-μm Millex-HV filters (MilliporeSigma, Burlingame, MA). The viruses were purified and concentrated about 1,000-fold by centrifugation at 90,000 g for 90 min. The virus titer was measured by infecting HEK293 cells with $10 \times$ gradient dilution (Chen et al., 2018; Li et al., 2016). Intrathecal catheters were inserted in rats during isoflurane-induced anesthesia as described before (Chen et al., 2000). The rats received a single intrathecal injection of 20 μL of the viral vector with 10^8 infectious units per mL. After vector injection, the intrathecal catheter was removed immediately, and all rats were placed in a restricted biohazard housing room for 2 weeks.

Immunoblotting and Immunoprecipitations—All the key reagents and antibodies used in this study are listed in Key Resources Table. We obtained protein samples from HEK293 cells and fresh dorsal spinal cord tissues at L5-L6 levels from anesthetized rats and frozen lumbar spinal cord tissues from 4 human donors (2 men and 2 women, age range 18–42 years, postmortem interval 17–29 h). HEK293 cells were transfected with

Lipofectamine 3000 (Invitrogen; 1:2.5 DNA/lipid) in Opti-MEM after they had grown to 80%–90% confluence in 75-cm^2 culture flasks. DNA amounts in each transfection were kept constant by the addition of empty vector. All experiments were conducted 48 h post-transfection. Cells were then washed 3 times in PBS and lysed in lysis buffer. The samples were homogenized in RIPA buffer containing (in mM) 50 Tris-HCl (pH 7.4), 1% NP-40, 0.1% SDS, 150 NaCl, 1 EDTA, 1 Na$_3$VO$_4$, and 1 NaF in the presence of a proteinase inhibitor cocktail (Sigma-Aldrich). The lysates were centrifuged at 13,000 rpm for 30 min at 4°C. The supernatant was carefully collected, and the protein concentration was measured using a DC Protein Assay Kit (Bio-Rad). A total of 30 μg of the total proteins from each sample was loaded and separated using 4%–15% Tris-HCl SDS-PAGE gels. The resolved proteins were transferred to an Immobilon-P membrane (MilliporeSigma). The membrane was treated with 5% nonfat dry milk in TBST at 25°C for 1 h and then incubated in TBS supplemented with 0.1% Triton X-100 and 1% BSA and primary antibodies overnight at 4°C. The membrane was washed three times and then incubated with horseradish peroxidase-conjugated secondary antibodies for 1 h at 25°C. The protein band was revealed using an ECL Plus Detection Kit (Thermo Fisher Scientific, Waltham, MA), and the protein band density was quantified with the Odyssey Fc Imager (LI-COR Biosciences, Lincoln, NE) and normalized to the control protein band on the same blot.

For immunoprecipitation (IP), the samples were resuspended and solubilized in IP buffer (50 mM Tris pH7.4, 250 mM NaCl, 10% glycerol, 0.5% NP-40, 20 mM NaF, 1 mM Na$_3$VO$_4$, 10 mM N-ethylmaleimide, 1 mM PMSF, 2 mM benzamide, and the protease inhibitor mixture), and the soluble fraction was incubated with protein A/G beads that pre-bound to the antibody at 4°C overnight. The protein A/G beads that pre-bound to mouse IgG or rabbit IgG were used as controls. Samples were immunoblotted after being washed three times with IP buffer. α2δ-1 was detected using rabbit anti-α2δ-1 antibody (#C5105, 1:1,000; Sigma-Aldrich), GluA1 was detected using mouse anti-GluA1 antibody (#75-327, 1:1,000; NeuroMab) or rabbit anti-GluA1 antibody (#ACC-015, 1:1,000; Alomone Labs), GluA2 was detected by using mouse anti-GluA2 antibody (#75-002, 1:1,000; NeuroMab) or rabbit anti-GluA2 antibody (#AGC-005, 1:1,000; Alomone Labs), and Flag Tag was detected using mouse anti-Flag antibody (#F1804, 1:1,000; Sigma-Aldrich) or rabbit anti-Flag antibody (#F7425, 1:1,000; Sigma-Aldrich).

Spinal Cord Synaptosome Preparation—The dorsal spinal cord at L5 and L6 was pooled from 4 SNL or sham rats and was homogenized using glass-Teflon homogenizer in 10 volumes of ice-cold HEPES-buffered sucrose (0.32 M sucrose, 1 mM EGTA, and 4 mM HEPES at pH 7.4) containing a protease inhibitor cocktail (Sigma-Aldrich). The homogenate was centrifuged at 1,000 g for 10 min at 4°C to remove the nuclei and large debris. The supernatant was centrifuged at 10,000 g for 15 min to obtain the crude synaptosomal fraction. The synaptosomal pellet was lysed via hypo-osmotic shock in 9 volumes of ice-cold HEPES buffer with the protease inhibitor cocktail for 30 min. The lysate was centrifuged at 25,000 g for 20 min at 4°C to obtain the synaptosomal membrane fraction (Chen et al., 2018, 2019b) for the following IP or immunoblotting experiments.

Cell Surface and Membrane Protein Isolation—HEK293 cells membrane surface proteins were isolated using Pierce Cell Surface Protein Isolation Kit (Thermo Fisher Scientific) according to the manufacturer's instruction. Briefly, the transfected cells (about 90% confluence) were incubated with Sulfo-NHS-SS-Biotin at 4°C for 30 min with gentle rotation. After the excess biotin was quenched with quenching solution, the cells were washed, harvested, and lysed with Lysis Buffer in a protease inhibitor cocktail for 30 min at 4°C. The lysates were then centrifuged at 10,000 g for 2 min at 4°C, and the supernatants were added to NeutrAvidin agarose and incubated for 60 min at 25°C with end-over-end mixing. The captured surface proteins were eluted from the Biotin-NeutrAvidin agarose by RIPA buffer for the immunoblotting analysis (Chen et al., 2018).

For obtaining plasma membrane protein extracts, transfected HEK293 cells were harvested and homogenized in ice-cold hypotonic buffer (20 mM Tris pH 7.4, 1 mM $CaCl_2$, 1 mM $MgCl_2$, and protease inhibitors). The nuclei and unbroken cells were removed by centrifugation at 300 g for 5 min, and the supernatant was centrifuged again for 20 min at 21,000 g. The pellets were resuspended and solubilized in IP buffer (50 mM Tris pH 7.4, 250 mM NaCl, 10% glycerol, 0.5% NP-40, 20 mM NaF, 1 mM Na_3VO_4, 10 mM N-ethylmaleimide, 1 mM PMSF, 2 mM benzamide, and the protease inhibitor cocktail).

Isolation of Endoplasmic Reticulum-Enriched Fraction—Isolation of the ER-enriched fraction was performed with Endoplasmic Reticulum Isolation Kit (Sigma-Aldrich). The transfected cells were trypsinized, centrifuged, and resuspended in 1 × hypotonic buffer (10 mM HEPES, 1 mM EGTA, and 25 mM KCl; pH 7.8). After 20 min of incubation on ice, the cells were centrifuged at 600 g for 5 min, and the supernatant was discarded. Cell pellets were incubated with 1 × Isotonic Extraction Buffer (10 mM HEPES, 250 mM sucrose, 1 mM EGTA, and 25 mM KCl; pH, 7.8) and passed 10 times through a 27-gauge needle. The homogenates were centrifuged at 1,000 g for 10 min at 4°C, and the resulting supernatant was recentrifuged at 12,000 g for 15 min at 4°C. This supernatant after mitochondrial fraction was centrifuged for 60 min at 100,000 g at 4°C. The resulting pellet (microsomal/ER fraction) was used for the blotting experiments.

For the dorsal spinal cord tissues, we added 10-fold 1 × Isotonic Extraction Buffer (10 mM HEPES, 250 mM sucrose, 1 mM EGTA, and 25 mM KCl; pH 7.8) and homogenized the sample using an overhead motor (about 200 rpm). The homogenate was centrifuged at 1,000 g for 10 min at 4°C, and the supernatant was re-centrifuged at 12,000 g for 15 min at 4°C. The supernatant, which is the post-mitochondrial fraction, was centrifuged again for 60 min at 100,000 g at 4°C. The resulting pellet was used for subsequent blotting and co-IP experiments.

Luminescence Resonance Energy Transfer Measurements—Luminescence Resonance Energy Transfer (LRET) measurements for constructs used for LRET measurements, the extracellular non–disulfide-bonded cysteines were mutated to serines so that they were not labeled with the maleimide reactive fluorophore. For measurement of LRET between GluA1 and α2δ-1, Ser-36 was mutated and was used as the site for attachment of the thiol-reactive fluorophore, and for LRET measurements between GluA2 and α2δ-1, Asp-23 (equivalent site to Ser-36 on GluA1) was mutated and was used as the

site for attachment of the thiol-reactive fluorophore. Additionally, for quantitative analysis of the background, a Factor Xa protease site (IDGR) was introduced at position 228 with the mutations T228I and D231R in GluA2 and at equivalent site in GluA1. Upon cleavage, the labeled amino-terminal domains dissociate, thus removing the specific AMPAR contribution to the LRET signal, thus providing the specific measurement of the LRET signal between the AMPAR and α2δ-1 (Chen et al., 2018). Cysteines at the GluA1 and GluA2 sites labeled with thiol-reactive terbium chelate served as donor fluorophore sites, and YFP fused to α2δ-1 served as the acceptor fluorophore. For measuring distance within the heteromer, cysteines at the GluA2 site labeled with thiol-reactive terbium chelate served as donor fluorophore sites, and GFP fused to the amino terminus of GluA1 served as the acceptor fluorophore. HEK293 cells transfected with respective constructs were harvested and labeled with 200 nM terbium chelate (Invitrogen) for 1 h at 25°C. After labeling, cells were washed twice in extracellular buffer composed of (in mM) 150 NaCl, 2.8 KCl, 1 CaCl$_2$, and 5 HEPES (pH 7.3). The washed and labeled cells were then re-suspended in extracellular buffer and probed in a cuvette-based Quanta-Master QM3-SS LRET system. The sample was excited at 337 nm, and emission was detected at 527 nm. The data were acquired with Fluorescan (Photon Technology International, Edison, NJ) and analyzed with Origin 8.6 software (OriginLab Corp., Northampton, MA). Each sample was scanned 3 times for each ligated condition, and each scan was recorded as an average of 99 sweeps. The distance between the donor and acceptor was calculated using the Förster equation.

LRET nano-positioning model of α2δ-1–GluA2 interaction was determined based on the distances obtained from LRET measurements (Chen et al., 2018; Shaikh et al., 2016). Spheres were drawn around the positions of the donor fluorophore on the GluA2 receptor using the LRET-determined distances as radii. Using the extracellular domain of the α2δ-1 structure (PDB: 5GJV, https://www.rcsb.org/structure/5gjv) (Wu et al., 2016) tagged with YFP at the N terminus, a series of rigid-body translations and rotations were performed to superpose the acceptor fluorophore on the plane of intersection of the donor fluorophore spheres, with the additional constraint of maintaining the C terminus of the extracellular domain of α2δ-1 near the membrane. The model that best fit the distance with minimal steric clashes positioned the extracellular domain of α2δ-1 next to the extracellular domains of the GluA2 receptor. While the precise location of α2δ-1 is difficult to predict based on the LRET distances, the LRET distance measurements indicate that it is near to and has extensive interactions with the extracellular domains of the GluA2 receptor. The electron microscopy structure of α2δ-1 ends at Cys-1071, and there is currently no structural information for the C terminus (residues beyond 1071) of α2δ-1.

***In Situ* Proximity Ligation Assay**—The proximity ligation assay (PLA) was performed according to the user guide for Duolink *In Situ* kit (Sigma-Aldrich). In brief, the cultured HEK293 cells or the rat spinal tissue slices were fixed with 4% paraformaldehyde for 10 min at 25°C and then blocked using the Blocking Solution in a pre-heated humidity chamber for 30 min at 37°C. After removing the Blocking Solution, we added the primary antibodies (mouse anti-GluA1, #75-327, NeuroMab; rabbit anti-GluA2, #AGC-005, Alomone Labs) diluted in the Antibody Diluent. After incubating the sample with primary antibodies in a humidity chamber overnight at 4°C, we washed the slides twice in 1 × Wash Buffer A

for 5 min. We then diluted the PLA probes in Antibody Diluent and incubated the slides in a humidity chamber for 1 h at 37°C. After washing the slides in 1 × Wash Buffer A for 2 × 5 min under gentle agitation, we added diluted Ligation-Ligase solution to the samples and incubated them in the humidity chamber for 30 min at 37°C. Next, we added the pre-diluted Amplification-Polymerase solution to each sample. Finally, the slides were washed and dried at 25°C in the dark and were mounted for imaging using a fluorescence microscope. The quantitative analysis of GluA1-GluA2 PLA signal particles in individual cells was performed using the NIH ImageJ Cell Counter Plugin.

Live Cell Calcium Imaging—HEK293 cells (ATCC, Manassas, VA) were maintained in Dulbecco's modified Eagle medium (DMEM) supplemented with 10% fetal bovine serum (#F4135, Sigma-Aldrich) and penicillin/streptomycin (#30-002-CI, Corning, Manassas, VA). When a confluence of 80%–90% was reached, the cells were passaged every 2 days. For cell transfection, 1.2×10^4 cells were plated on poly-D-lysine–coated coverslips in each well of a 24-well plate. After 24 h, PolyJet reagents (#SL100688, SignaGen Laboratories, Rockville, MD) were used to transfect the cells with GCaMP6, an ultrasensitive calcium sensor, with GluA1 and GluA2 (ratio of 1:1:1) or GCaMP6/GluA1/GluA2/α2δ-1 (ratio of 1:1:1:2) with a 1:3 ratio of DNA:PolyJet. The GCaMP6 plasmid was obtained from Addgene. Five h later, transfected cells were cultured in glutamate-free DMEM for another 19-24 h before final imaging experiments.

Live cell imaging was conducted using an inverted microscope. Glass coverslips with adhering cells were held in a chamber (0.5 mL volume) that was superfused continuously (1.0 ml/min) with solution containing 110 mM N-methyl-D-glucamine, 5 mM HEPES, and 30 mM $CaCl_2$ (pH 7.4 adjusted with HCl; osmolality, 310 mOsm). Cyclothiazide (100 μM) was included in the extracellular solution. GCaMP-positive cells were first identified under epifluorescent illumination. GCaMP fluorescence signals (excitation 485 nm, 5 nm bandpass; emission 510 nm) were captured via a digital camera. The fluorescence signals of cells within a viewing field were recorded and presented as the change in fluorescence intensity normalized by the baseline (F/F0).

Electrophysiological Recordings in HEK293 Cells—For transfection, 1.2×10^4 cells were plated on poly-D-lysine coated coverslips in each well of a 24-well plate. DNA for GluA1, GluA2 (R or Q), or GluA1 plus GluA2 (R or Q) was transfected either alone or with α2δ-1. Coexpression of GFP was used to identify transfected cells. The transfection ratio of GluA1, GluA2 and α2δ-1 was 1:1:2 using PolyJet DNA *In Vitro* Transfection Reagent. After 4 h of transfections, we replaced the culture medium with new glutamine-free medium. Electrophysiological recordings were performed 24–48 h after transfection.

Whole-cell recordings were performed using an EPC-10 amplifier (HEKA Instruments, Lambrecht, Germany). The current-voltage relationship of glutamate-elicited currents was determined using a voltage ramp from −80 mV to 70 mV at 100 mV/s. The rectification index was calculated by dividing the current amplitude recorded at +50 mV by that at −50 mV. The extracellular recording solution consisted of (in mM) 145 NaCl, 2.5 KCl, 1 $CaCl_2$, 1 $MgCl_2$, 10 glucose, and 10 HEPES (pH 7.3; osmolarity, 320 mOsm). Electrodes (resistance, 4–6 MΩ) were filled with pipette solution (in mM) 145 CsCl, 2.5 NaCl, 10

HEPES, 1 EGTA, 4 MgATP, and 0.1 spermine tetrahydrochloride (pH 7.3; osmolarity, 300 mOsm). The cell membrane capacitance and series resistance were electronically compensated. Glutamate (1 mM) plus cyclothiazide (50 μM, Tocris Bioscience, Bristol, UK) was used for measurements of relative calcium permeability, and 10 mM glutamate plus 100 μM cyclothiazide was used for other experiments.

Measurement of relative calcium permeability was carried out as described previously (Soto et al., 2007). In brief, a voltage ramp from −80 to 70 mV was applied in "low" and "high" Ca^{2+} solutions. Low-Ca^{2+} solution (in mM) comprised 145 NaCl, 2.5 KCl, 1 $CaCl_2$, 1 $MgCl_2$, and 10 HEPES; high-Ca^{2+} solution comprised 30 $CaCl_2$, 110 N-methyl-D-glucamine, 5 HEPES, and 50 sucrose. The relative Ca^{2+} permeability, P_{Ca}/P_{Na}, was determined from the reversal potentials in low-Ca^{2+} and high-Ca^{2+} solutions using the equation: $P_{Ca}/P_{Na} = a_{Na}/4a_{Ca}(\exp[(2V_{revCa} - V_{revNa})F)/RT]+ \exp[(V_{revCa} − V_{revNa})F)/RT])$, where a_{Na} and a_{Ca} represent the activities of Na^+ and Ca^{2+} in the extracellular solutions. R, T, and F denote the gas constant, temperature in degrees Kelvin, and Faraday constant, respectively.

Electrophysiological Recordings in Spinal Cord Slices—Whole-cell patch-clamp recordings were performed in spinal cord slices at the L5 and L6 levels. We removed the lumbar spinal cord through laminectomy in rats or mice during isoflurane-induced anesthesia. The spinal cords were placed in ice-cold sucrose artificial cerebrospinal fluid containing (in mM) 234 sucrose, 3.6 KCl, 1.2 $MgCl_2$, 2.5 $CaCl_2$, 1.2 NaH_2PO_4, 12.0 glucose, and 25.0 $NaHCO_3$, presaturated with 95% O_2 and 5% CO_2. We sliced the spinal cord (400 μm) using a vibratome slicer and continuously superfused the slices with artificial cerebrospinal fluid.

Neurons in the lamina II outer zone of the spinal cord were identified with the use of differential interference contrast/infrared illumination on a fixed-stage microscope (BX50WI; Olympus, Tokyo, Japan). The borosilicate pipettes were filled with a solution containing (in mM) 110 Cs_2SO_4, 5 TEA, 2.0 $MgCl_2$, 0.5 $CaCl_2$, 5.0 HEPES, 5.0 EGTA, 5.0 ATP-Mg, 0.5 Na-GTP, 0.1 spermine, and 10 lidocaine N-ethyl bromide (adjusted to pH 7.2–7.4 with 1 M CsOH, 290–300 mOsm). We included 0.1 mM spermine in the intracellular solution to compensate for a possible loss of endogenous polyamines from intracellular dialysis during whole-cell recordings (Chen et al., 2013a). Monosynaptic excitatory postsynaptic currents (EPSCs) were elicited by electrical stimulation (0.2 ms, 0.4–0.8 mA, and 0.1 Hz) of the dorsal root and recorded at holding potentials from −70 to +70 mV. The rectification index was calculated by dividing the amplitude of AMPAR-EPSCs recorded at +50 mV by that at −50 mV. Monosynaptic EPSCs were identified on the basis of the constant latency and absence of conduction failure of evoked EPSCs in response to a 20-Hz electrical stimulation (Chen et al., 2018; Zhou et al., 2010). The input resistance was continuously monitored, and the recording was terminated if the input resistance changed by more than 15%.

To determine whether nerve injury increases presynaptic CP-AMPAR activity at central terminals of dorsal root ganglion neurons, we performed whole-cell recording of AMPAR-EPSCs monosynaptically evoked from dorsal root stimulation. The postsynaptic CP-

AMPARs of dorsal horn neurons were blocked first via intracellular dialysis of 10 mM IEM-1460 (included in the pipette recording solution), a selective CP-AMPAR open-channel blocker (Sebe et al., 2017; Twomey et al., 2018). Because IEM-1460 was slowly dialyzed via a small tip of a recording pipette, the concentration of IEM-1460 was 100-fold higher in the pipette solution than in the bath solution, based our experience of blocking postsynaptic NMDARs in dorsal horn neurons (Zhou et al., 2010). In this experimental setting, a reduction in the amplitude of evoked AMPAR-EPSCs by subsequent bath application of 100 µM IEM-1460 would suggest a role of presynaptic CP-AMPARs in regulating glutamate release from primary afferent nerve terminals.

QUANTIFICATION AND STATISTICAL ANALYSIS

Data are presented as means ± SEM. The protein band density was quantified and normalized to the control protein band on the same blot. The evoked EPSCs were analyzed using Clampfit 10.0 software (Axon Instruments). The rectification index was calculated by dividing the current amplitude recorded at +50 mV by that at −50 mV. We used a two-tailed Student t test to compare two groups and one-way or two-way analysis of variance (ANOVA, followed by Dunnett's or Tukey's post hoc test) to compare more than two groups. We used the appropriate nonparametric analysis (i.e., the Mann-Whitney U test or Kruskal-Wallis test) when electrophysiological and biochemical data were not normally distributed. The statistical details of experiments and p values were described in the figures and figure legends. Statistical analyses were performed using Prism 8 software (GraphPad Software Inc., San Diego, CA). The level of significance was set at $p < 0.05$.

Supplementary Material

Refer to Web version on PubMed Central for supplementary material.

ACKNOWLEDGMENTS

REFERENCES

Bowie D, and Mayer ML (1995). Inward rectification of both AMPA and kainate subtype glutamate receptors generated by polyamine-mediated ion channel block. Neuron 15, 453–462. [PubMed: 7646897]

Burnashev N, Monyer H, Seeburg PH, and Sakmann B (1992). Divalent ion permeability of AMPA receptor channels is dominated by the edited form of a single subunit. Neuron 8, 189–198. [PubMed: 1370372]

Chaplan SR, Bach FW, Pogrel JW, Chung JM, and Yaksh TL (1994). Quantitative assessment of tactile allodynia in the rat paw. J. Neurosci. Methods 53, 55–63. [PubMed: 7990513]

Chen SR, Eisenach JC, McCaslin PP, and Pan HL (2000). Synergistic effect between intrathecal non-NMDA antagonist and gabapentin on allodynia induced by spinal nerve ligation in rats. Anesthesiology 92, 500–506. [PubMed: 10691238]

Chen SR, Zhou HY, Byun HS, and Pan HL (2013a). Nerve injury increases GluA2-lacking AMPA receptor prevalence in spinal cords: functional significance and signaling mechanisms. J. Pharmacol. Exp. Ther 347, 765–772. [PubMed: 24030012]

Chen TW, Wardill TJ, Sun Y, Pulver SR, Renninger SL, Baohan A, Schreiter ER, Kerr RA, Orger MB, Jayaraman V, et al. (2013b). Ultrasensitive fluorescent proteins for imaging neuronal activity. Nature 499, 295–300. [PubMed: 23868258]

Chen SR, Zhou HY, Byun HS, Chen H, and Pan HL (2014). Casein kinase II regulates N-methyl-D-aspartate receptor activity in spinal cords and pain hypersensitivity induced by nerve injury. J. Pharmacol. Exp. Ther 350, 301–312. [PubMed: 24898266]

Chen J, Li L, Chen SR, Chen H, Xie JD, Sirrieh RE, MacLean DM, Zhang Y, Zhou MH, Jayaraman V, and Pan HL (2018). The α2δ-1-NMDA Receptor Complex Is Critically Involved in Neuropathic Pain Development and Gabapentin Therapeutic Actions. Cell Rep. 22, 2307–2321. [PubMed: 29490268]

Chen SR, Zhang J, Chen H, and Pan HL (2019a). Streptozotocin-Induced Diabetic Neuropathic Pain Is Associated with Potentiated Calcium-Permeable AMPA Receptor Activity in the Spinal Cord. J. Pharmacol. Exp. Ther 371, 242–249. [PubMed: 31481518]

Chen Y, Chen SR, Chen H, Zhang J, and Pan HL (2019b). Increased α2δ-1-NMDA receptor coupling potentiates glutamatergic input to spinal dorsal horn neurons in chemotherapy-induced neuropathic pain. J. Neurochem 148, 252–274. [PubMed: 30431158]

Cole RL, Lechner SM, Williams ME, Prodanovich P, Bleicher L, Varney MA, and Gu G (2005). Differential distribution of voltage-gated calcium channel alpha-2 delta (alpha2delta) subunit mRNA-containing cells in the rat central nervous system and the dorsal root ganglia. J. Comp. Neurol 491, 246–269. [PubMed: 16134135]

Conrad KL, Tseng KY, Uejima JL, Reimers JM, Heng LJ, Shaham Y, Marinelli M, and Wolf ME (2008). Formation of accumbens GluR2-lacking AMPA receptors mediates incubation of cocaine craving. Nature 454, 118–121. [PubMed: 18500330]

El-Awaad E, Pryymachuk G, Fried C, Matthes J, Isensee J, Hucho T, Neiss WF, Paulsson M, Herzig S, Zaucke F, and Pietsch M (2019). Direct, gabapentin-insensitive interaction of a soluble form of the calcium channel subunit $\alpha_2\delta$-1 with thrombospondin-4. Sci. Rep 9, 16272. [PubMed: 31700036]

Field MJ, Cox PJ, Stott E, Melrose H, Offord J, Su TZ, Bramwell S, Corradini L, England S, Winks J, et al. (2006). Identification of the alpha2delta-1 subunit of voltage-dependent calcium channels as a molecular target for pain mediating the analgesic actions of pregabalin. Proc. Natl. Acad. Sci. USA 103, 17537–17542. [PubMed: 17088553]

Friedman LK, and Koudinov AR (1999). Unilateral GluR2(B) hippocampal knockdown: a novel partial seizure model in the developing rat. J. Neurosci 19, 9412–9425. [PubMed: 10531445]

Fuller-Bicer GA, Varadi G, Koch SE, Ishii M, Bodi I, Kadeer N, Muth JN, Mikala G, Petrashevskaya NN, Jordan MA, et al. (2009). Targeted disruption of the voltage-dependent calcium channel alpha2/delta-1-subunit. Am. J. Physiol. Heart Circ. Physiol 297, H117–H124. [PubMed: 19429829]

Greger IH, Khatri L, and Ziff EB (2002). RNA editing at arg607 controls AMPA receptor exit from the endoplasmic reticulum. Neuron 34, 759–772. [PubMed: 12062022]

Greger IH, Khatri L, Kong X, and Ziff EB (2003). AMPA receptor tetramerization is mediated by Q/R editing. Neuron 40, 763–774. [PubMed: 14622580]

He XY, Li YJ, Kalyanaraman C, Qiu LL, Chen C, Xiao Q, Liu WX, Zhang W, Yang JJ, Chen G, et al. (2016). GluA1 signal peptide determines the spatial assembly of heteromeric AMPA receptors. Proc. Natl. Acad. Sci. USA 113, E5645–E5654. [PubMed: 27601647]

Henley JM, and Wilkinson KA (2016). Synaptic AMPA receptor composition in development, plasticity and disease. Nat. Rev. Neurosci 17, 337–350. [PubMed: 27080385]

Huang Y, Chen SR, Chen H, Luo Y, and Pan HL (2020). Calcineurin Inhibition Causes α2δ-1-Mediated Tonic Activation of Synaptic NMDA Receptors and Pain Hypersensitivity. J. Neurosci 40, 3707–3719. [PubMed: 32269108]

Isaac JT, Ashby MC, and McBain CJ (2007). The role of the GluR2 subunit in AMPA receptor function and synaptic plasticity. Neuron 54, 859–871. [PubMed: 17582328]

Kobylecki C, Cenci MA, Crossman AR, and Ravenscroft P (2010). Calcium-permeable AMPA receptors are involved in the induction and expression of l-DOPA-induced dyskinesia in Parkinson's disease. J. Neurochem 114, 499–511. [PubMed: 20456008]

Kuniishi H, Yamada D, Wada K, Yamada M, and Sekiguchi M (2020). Stress induces insertion of calcium-permeable AMPA receptors in the OFC-BLA synapse and modulates emotional behaviours in mice. Transl. Psychiatry 10, 154. [PubMed: 32424318]

Li DP, Byan HS, and Pan HL (2012). Switch to glutamate receptor 2-lacking AMPA receptors increases neuronal excitability in hypothalamus and sympathetic drive in hypertension. J. Neurosci 32, 372–380. [PubMed: 22219297]

Li L, Chen SR, Chen H, Wen L, Hittelman WN, Xie JD, and Pan HL (2016). Chloride Homeostasis Critically Regulates Synaptic NMDA Receptor Activity in Neuropathic Pain. Cell Rep. 15, 1376–1383. [PubMed: 27160909]

Lu W, Shi Y, Jackson AC, Bjorgan K, During MJ, Sprengel R, Seeburg PH, and Nicoll RA (2009). Subunit composition of synaptic AMPA receptors revealed by a single-cell genetic approach. Neuron 62, 254–268. [PubMed: 19409270]

Luo ZD, Calcutt NA, Higuera ES, Valder CR, Song YH, Svensson CI, and Myers RR (2002). Injury type-specific calcium channel alpha 2 delta-1 subunit up-regulation in rat neuropathic pain models correlates with antiallodynic effects of gabapentin. J. Pharmacol. Exp. Ther 303, 1199–1205. [PubMed: 12438544]

Mayer ML (2006). Glutamate receptors at atomic resolution. Nature 440, 456–462. [PubMed: 16554805]

Noh KM, Yokota H, Mashiko T, Castillo PE, Zukin RS, and Bennett MV (2005). Blockade of calcium-permeable AMPA receptors protects hippocampal neurons against global ischemia-induced death. Proc. Natl. Acad. Sci. USA 102, 12230–12235. [PubMed: 16093311]

Rock DM, Kelly KM, and Macdonald RL (1993). Gabapentin actions on ligand- and voltage-gated responses in cultured rodent neurons. Epilepsy Res. 16, 89–98. [PubMed: 7505742]

Rosenstock J, Tuchman M, LaMoreaux L, and Sharma U (2004). Pregabalin for the treatment of painful diabetic peripheral neuropathy: a double-blind, placebo-controlled trial. Pain 110, 628–638. [PubMed: 15288403]

Rossmann M, Sukumaran M, Penn AC, Veprintsev DB, Babu MM, and Greger IH (2011). Subunit-selective N-terminal domain associations organize the formation of AMPA receptor heteromers. EMBO J. 30, 959–971. [PubMed: 21317873]

Sebe JY, Cho S, Sheets L, Rutherford MA, von Gersdorff H, and Raible DW (2017). Ca^{2+}-Permeable AMPARs Mediate Glutamatergic Transmission and Excitotoxic Damage at the Hair Cell Ribbon Synapse. J. Neurosci 37, 6162–6175. [PubMed: 28539424]

Shaikh SA, Dolino DM, Lee G, Chatterjee S, MacLean DM, Flatebo C, Landes CF, and Jayaraman V (2016). Stargazin Modulation of AMPA Receptors. Cell Rep. 17, 328–335. [PubMed: 27705782]

Sommer B, Köhler M, Sprengel R, and Seeburg PH (1991). RNA editing in brain controls a determinant of ion flow in glutamate-gated channels. Cell 67, 11–19. [PubMed: 1717158]

Soto D, Coombs ID, Kelly L, Farrant M, and Cull-Candy SG (2007). Stargazin attenuates intracellular polyamine block of calcium-permeable AMPA receptors. Nat. Neurosci 10, 1260–1267. [PubMed: 17873873]

Studniarczyk D, Coombs I, Cull-Candy SG, and Farrant M (2013). TARP γ-7 selectively enhances synaptic expression of calcium-permeable AMPARs. Nat. Neurosci 16, 1266–1274. [PubMed: 23872597]

Tétreault MP, Bourdin B, Briot J, Segura E, Lesage S, Fiset C, and Parent L (2016). Identification of Glycosylation Sites Essential for Surface Expression of the CaVα2δ1 Subunit and Modulation of the Cardiac CaV1.2 Channel Activity. J. Biol. Chem 291, 4826–4843. [PubMed: 26742847]

Tomita S, Adesnik H, Sekiguchi M, Zhang W, Wada K, Howe JR, Nicoll RA, and Bredt DS (2005). Stargazin modulates AMPA receptor gating and trafficking by distinct domains. Nature 435, 1052–1058. [PubMed: 15858532]

Traynelis SF, Wollmuth LP, McBain CJ, Menniti FS, Vance KM, Ogden KK, Hansen KB, Yuan H, Myers SJ, and Dingledine R (2010). Glutamate receptor ion channels: structure, regulation, and function. Pharmacol. Rev 62, 405–496. [PubMed: 20716669]

Twomey EC, Yelshanskaya MV, Vassilevski AA, and Sobolevsky AI (2018). Mechanisms of Channel Block in Calcium-Permeable AMPA Receptors. Neuron 99, 956–968.e4. [PubMed: 30122377]

Wenthold RJ, Petralia RS, Blahos J II, and Niedzielski AS (1996). Evidence for multiple AMPA receptor complexes in hippocampal CA1/CA2 neurons. J. Neurosci 16, 1982–1989. [PubMed: 8604042]

Whitehead G, Regan P, Whitcomb DJ, and Cho K (2017). Ca^{2+}-permeable AMPA receptor: A new perspective on amyloid-beta mediated pathophysiology of Alzheimer's disease. Neuropharmacology 112 (Pt A), 221–227. [PubMed: 27561971]

Wu J, Yan Z, Li Z, Qian X, Lu S, Dong M, Zhou Q, and Yan N (2016). Structure of the voltage-gated calcium channel Ca(v)1.1 at 3.6 Å resolution. Nature 537, 191–196. [PubMed: 27580036]

Xia J, Zhang X, Staudinger J, and Huganir RL (1999). Clustering of AMPA receptors by the synaptic PDZ domain-containing protein PICK1. Neuron 22, 179–187. [PubMed: 10027300]

Zhou HY, Chen SR, Chen H, and Pan HL (2010). Opioid-induced long-term potentiation in the spinal cord is a presynaptic event. J. Neurosci 30, 4460–4466. [PubMed: 20335482]

Zhou HY, Chen SR, Byun HS, Chen H, Li L, Han HD, Lopez-Berestein G, Sood AK, and Pan HL (2012). N-methyl-D-aspartate receptor- and calpain-mediated proteolytic cleavage of K+-Cl–cotransporter-2 impairs spinal chloride homeostasis in neuropathic pain. J. Biol. Chem 287, 33853–33864. [PubMed: 22854961]

Highlights

- Nerve injury augments postsynaptic Ca^{2+}-permeable AMPARs in the spinal cord via α2δ-1

- α2δ-1, but not α2δ-2 or α2δ-3, interacts directly with GluA1 and GluA2 via its C terminus

- α2δ-1 disrupts heteromeric, but not homomeric, assembly of GluA1 and GluA2 in the ER

- Gabapentin restores assembly and synaptic expression of GluA1/GluA2 in neuropathic pain
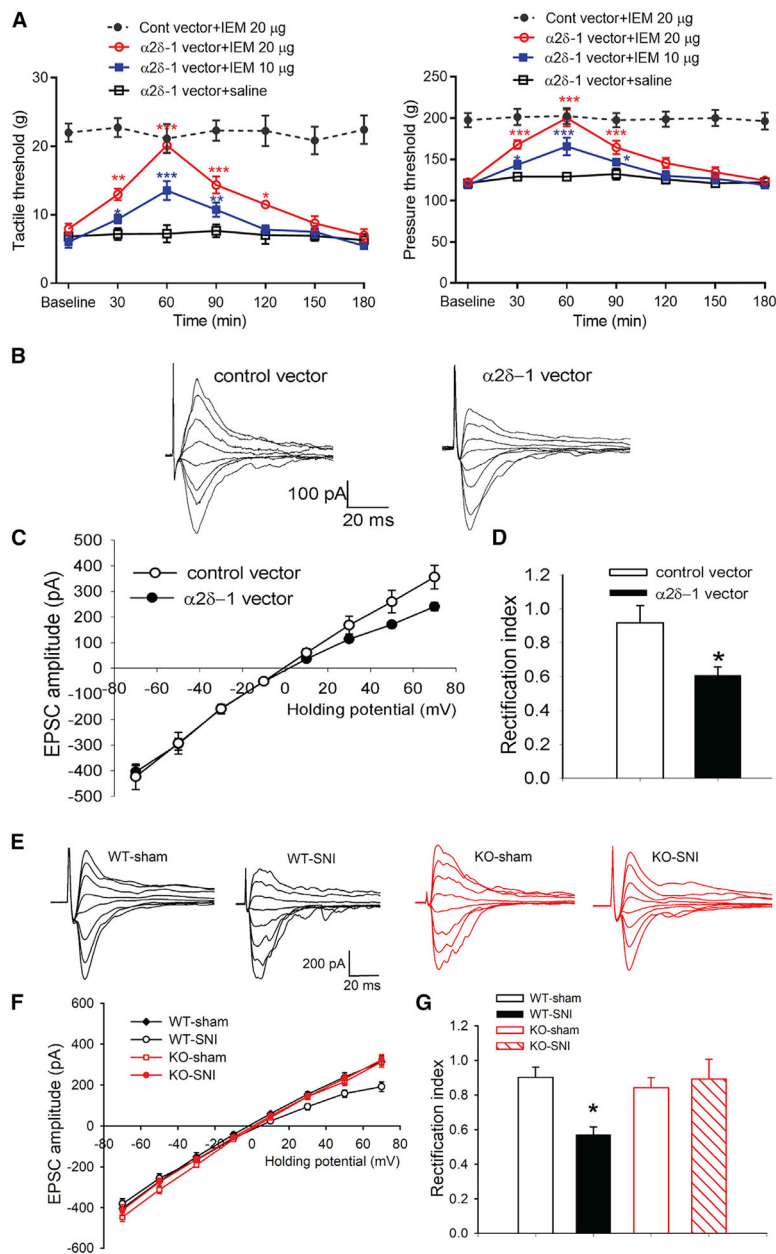
Figure 1. α2δ-1 is essential for the increased prevalence of CP-AMPARs in spinal cord synapses in neuropathic pain

(A) Effect of intrathecal injection of 10 and 20 μg of IEM-1460 (IEM) on the withdrawal thresholds in rats treated with a lentiviral *Cacna2d1* (α2δ-1) vector (n = 9 rats) or a control (Cont) vector (n = 8 rats). *p < 0.05, **p < 0.01, ***p < 0.001 versus baseline. One-way ANOVA followed by Dunnett test.

(B–D) α2δ-1 overexpression induces a switch from CI-AMPARs to CP-AMPARs in spinal dorsal horn neurons. Original traces (B), I-V plots (C), and rectification index (D) of AMPAR-EPSCs of neurons in rats 5 weeks after injection of a lentiviral *Cacna2d1* vector (n = 15 neurons) or a control vector (n = 11 neurons). *p < 0.05 versus the control vector (two-tailed Student's t test).

(E–G) Nerve injury has no effect on AMPARs in spinal dorsal horn neurons of *Cacna2d1* knockout (KO) mice. Original traces (E), I-V plots (F), and rectification index (G) of AMPAR-EPSCs of lamina II neurons in wild-type (WT) and *Cacna2d1* KO mice subjected to spared nerve injury (SNI; n = 15 neurons in WT, n = 13 neurons in *Cacna2d1* KO) or sham surgery (n = 14 neurons in WT, n = 13 neurons in KO). *p < 0.05 versus WT sham group. One-way ANOVA followed by Tukey test.
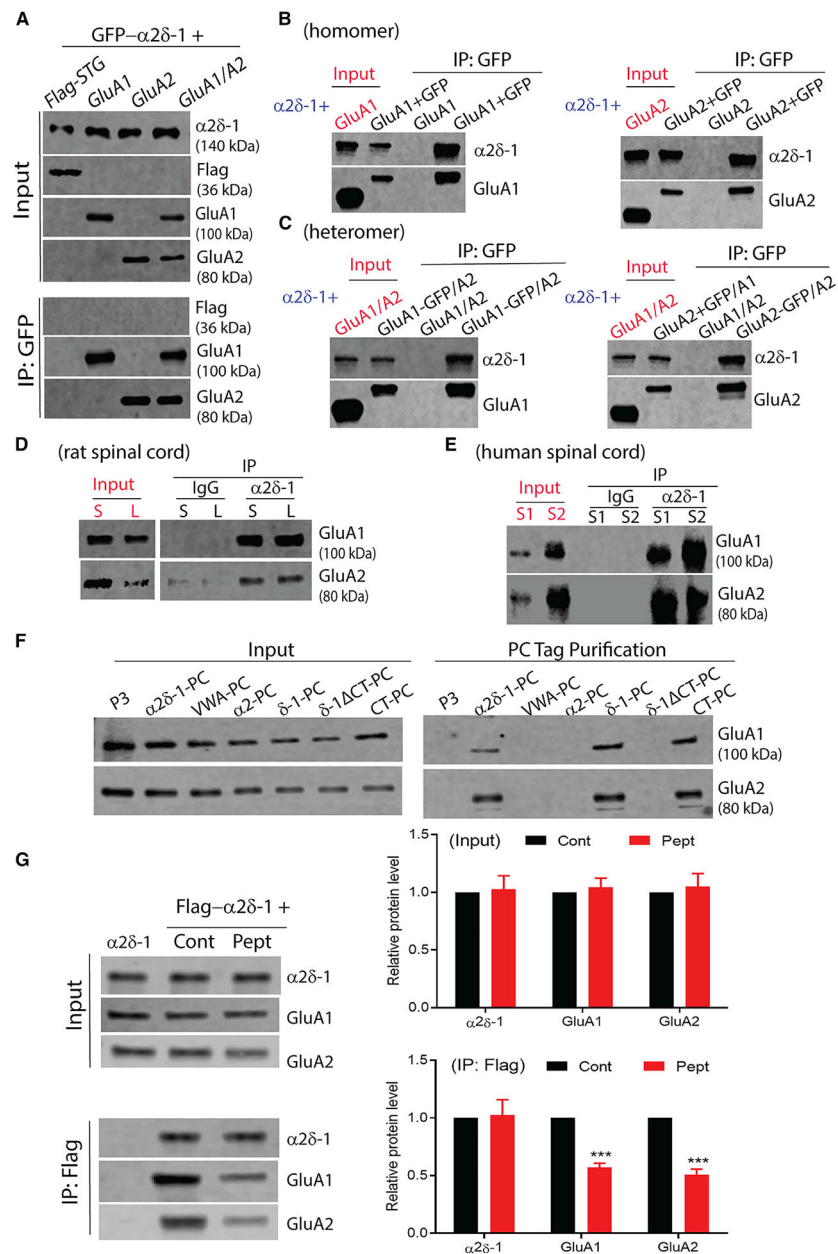
Figure 2. α2δ-1 physically interacts with GluA1 and GluA2 *in vitro* and *in vivo*

(A) CoIP shows the interaction between α2δ-1 and GluA1 and GluA2 in HEK293 cells. Cells cotransfected with GFP-tagged α2δ-1 and GluA1, GluA2, GluA1/GluA2, or FLAG-stargazin (STG).

(B) CoIP shows the interaction of α2δ-1 with homomeric GluA1 or GluA2 in HEK293 cells. P3, control vector.

(C) CoIP shows the interaction of α2δ-1 with heteromeric GluA1/GluA2 in HEK293 cells.

(D) CoIP shows the interaction of α2δ-1 with GluA1 and GluA2 in the dorsal spinal cord of rats subjected to a sham procedure (S) or spinal nerve ligation (L).

(E) CoIP shows the interaction of α2δ-1 with GluA1 and GluA2 subunits in the normal spinal cord tissue of two human donors (S1 and S2).

(F) α2δ-1 interacts with GluA1 and GluA2 subunits via its C terminus. HEK293 cells were cotransfected with GluA1/GluA2 and various PC-tagged α2δ-1 constructs. δ-1 CT, δ-1 without the C terminus; CT, the C terminus of δ-1; VWA, von Willebrand factor type A domain.

(G) CoIP shows that α2δ-1CT-Tat peptide disrupts the α2δ-1 interaction with GluA1 and GluA2 in HEK293 cells. Cell were cotransfected with GluA1/GluA2 and α2δ-1 or FLAG-α2δ-1 and were treated with 1 μM α2δ-1CT-Tat peptide (Pept) or 1 μM Tat-fused Cont peptide for 30 min. ***p < 0.001 versus the control peptide group (n = 5 samples per group, Mann-Whitney U test).

Experiments were repeated 3 times (F), 4 times (A, D, and E), or 5 times (B and C).
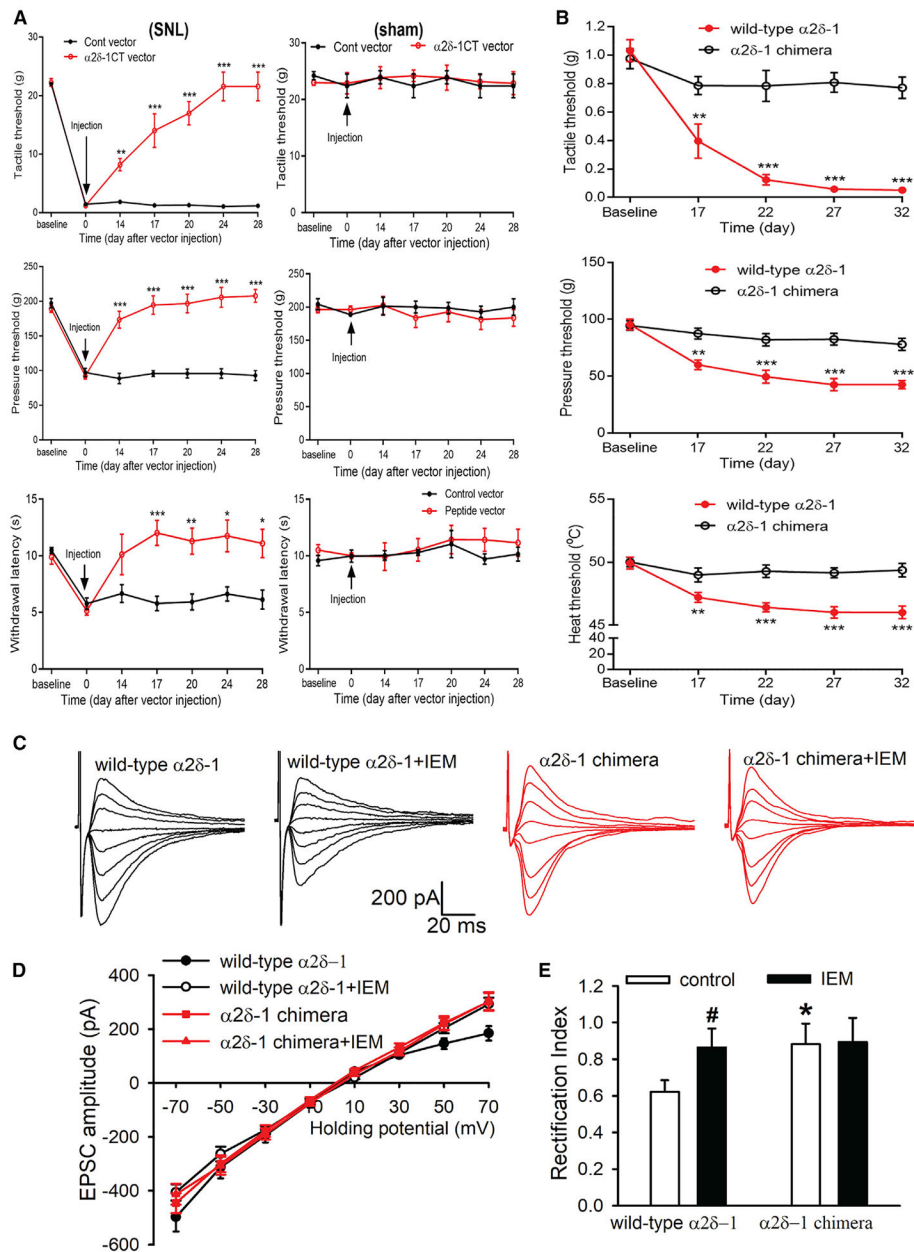
Figure 3. α2δ-1's C terminus is critically involved in the dominance of synaptic CP-AMPARs in spinal cords in neuropathic pain

(A) Effect of lentiviral vector-mediated expression of the α2δ-1 C terminus peptide on nerve-injury-induced chronic pain in rats. The lentiviral vector expressing the C-terminal sequence of α2δ-1 (CT vector, n = 8 rats) and a Cont vector (n = 7 rats) were intrathecally injected in rats 2 weeks after spinal nerve ligation (SNL). *p < 0.05, **p < 0.01, ***p < 0.001 versus baselines. One-way ANOVA followed by Dunnett test.

(B) Effect of intrathecal injection of a lentiviral vector expressing wild-type α2δ-1 or α2δ-1 chimera (α2δ-1$_{CT(α2δ-3)}$) vector on withdrawal thresholds in *Cacna2d1* KO mice (n = 10 mice per group). **p < 0.01, ***p < 0.001 versus baselines. One-way ANOVA followed by Dunnett test.

(C–E) Original traces (C), I-V plots (D), and rectification index (E) of AMPAR-EPSCs of lamina II neurons before and during bath application of 100 μM IEM-1460. AMPAR-EPSCs were recorded in *Cacna2d1* KO mice 5 weeks after intrathecal injection of a lentiviral vector expressing wild-type α2δ-1 (n = 15 neurons) or α2δ-1 chimera (α2δ-1$_{CT(α2δ-3)}$, n = 16 neurons). *p < 0.05 versus the wild-type α2δ-1 vector group; #p < 0.05 versus baseline control. One-way ANOVA followed by Tukey test.
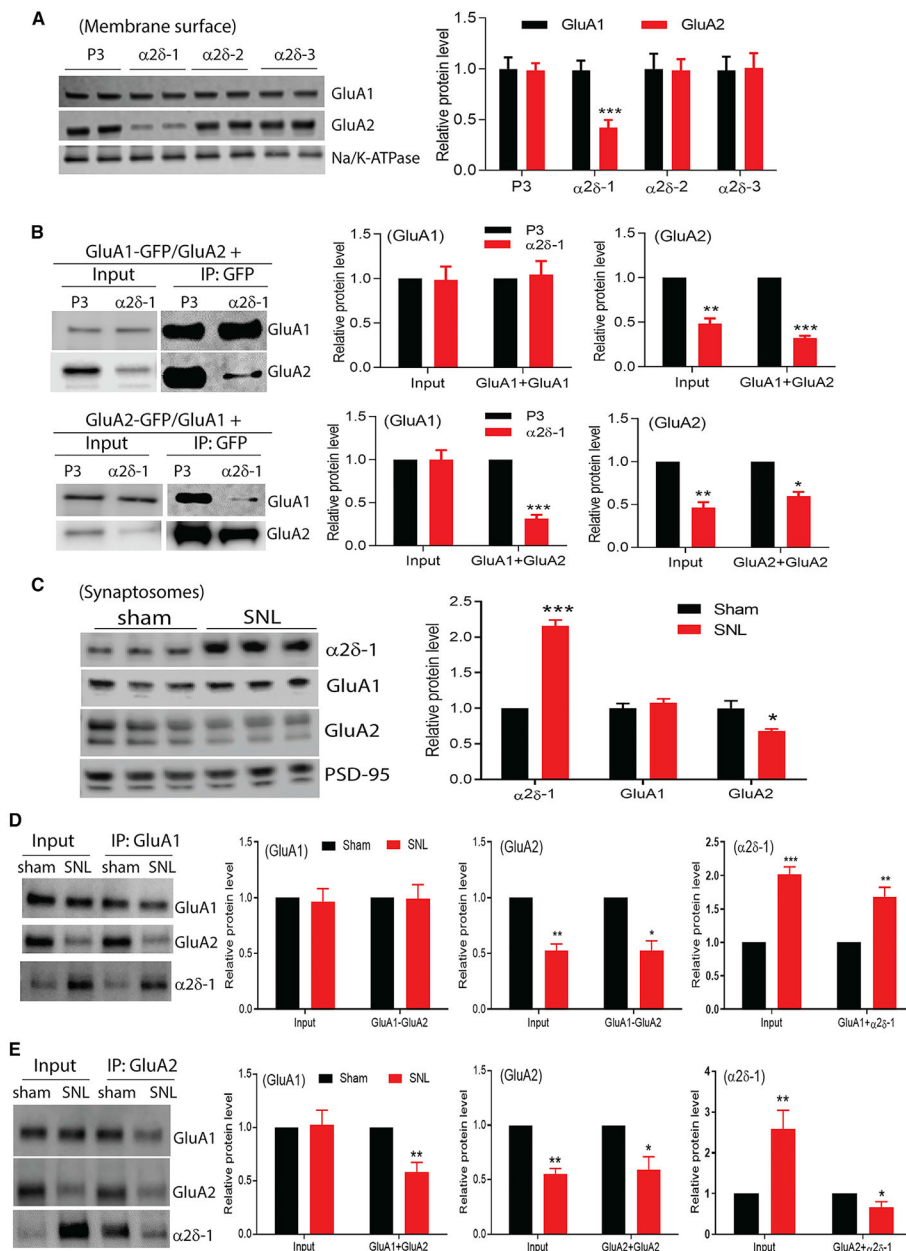
Figure 4. α2δ-1 reduces surface and synaptic expression of GluA2 and heteromeric GluA1/GluA2 receptors

(A) Original blots and quantification show the protein levels of GluA1 and GluA2 in HEK293 cells cotransfected with GluA1/GluA2 and control vector (pcDNA3, P3), α2δ-1, α2δ-2, or α2δ-3 (n = 4 per group). ***p < 0.001 versus the control vector group.

(B) Original blots and quantification show that α2δ-1 reduces cell membrane expression of heteromeric GluA1/GluA2 receptors in HEK293 cells. Surface membrane proteins were isolated by biotinylation and were precipitated with an anti-GFP antibody (n = 4 per group). *p < 0.05, **p < 0.01, ***p < 0.001 versus the P3 group.

(C) Original blots and quantification show that nerve injury increases α2δ-1 but reduces GluA2 in spinal cord synaptosomes (n = 5 rats per group). *p < 0.05, ***p < 0.001 versus the sham group.

(D and E) Original blots and quantification show that nerve injury reduces heteromeric GluA1/GluA2 receptors in spinal cord synaptosomes (n = 5 rats per group). *p < 0.05, **p < 0.01, ***p < 0.001 versus the sham group.

Mann-Whitney U test was conducted in (A)–(E).
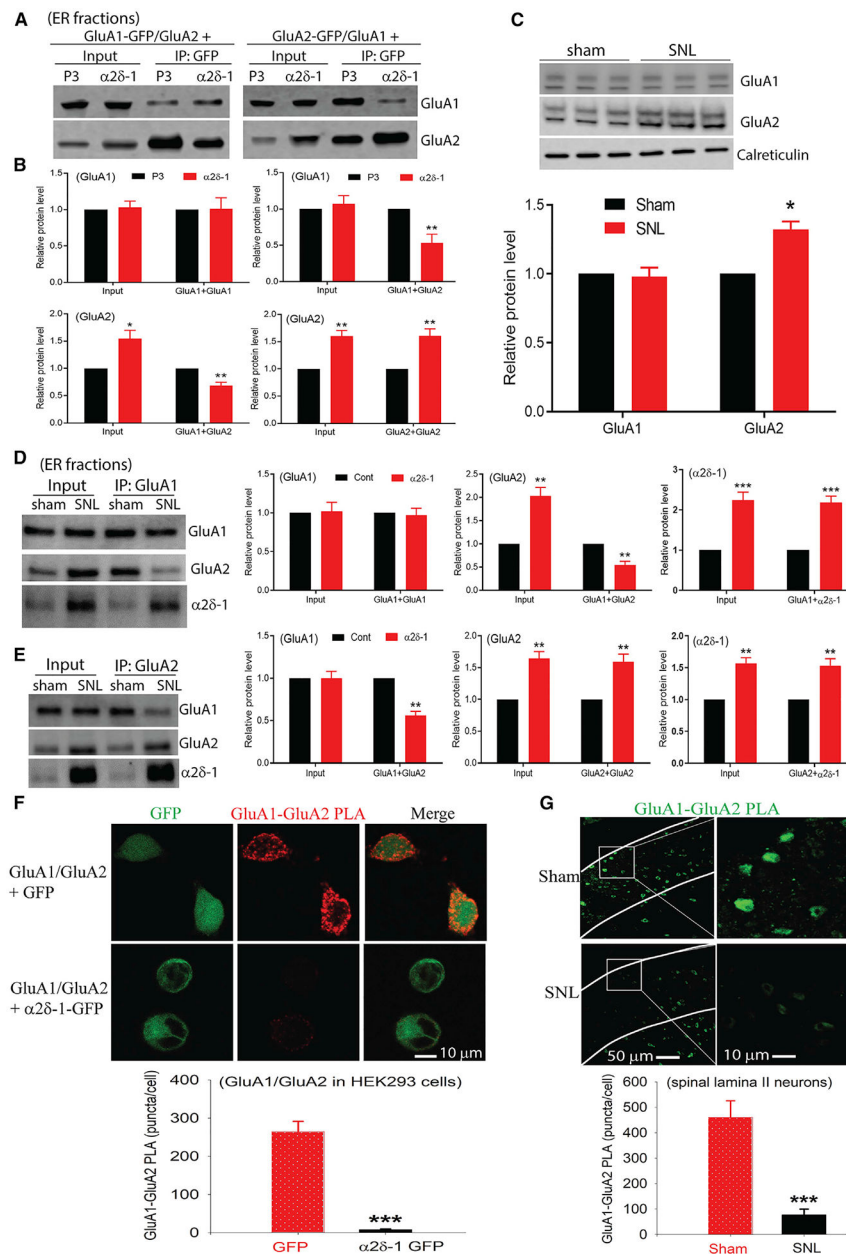
Figure 5. α2δ-1 disrupts the heteromeric assembly of GluA1/GluA2 and increases GluA2 retention in the endoplasmic reticulum

(A and B) Original blots (A) and quantification (B) show that α2δ-1 coexpression diminishes heteromeric GluA1/GluA2 receptors in the ER of HEK293 cells. n = 5 per group. *p < 0.05, **p < 0.01 versus the control vector group.

(C) Original blots and quantification show that nerve injury increases GluA2 retention in the ER of the spinal cord. ER-enriched fractions were isolated from dorsal spinal cords of sham control and SNL rats 3 weeks after surgery. Blotting was conducted using antibodies against GluA1, GluA2, and calreticulin (an ER protein marker). n = 5 rats per group. *p < 0.05 versus the sham group.

(D and E) Original blots and quantification show that nerve injury diminishes heteromeric GluA1/GluA2 receptors in the ER extracts of spinal cords. n = 5 rats per group. **p < 0.01, ***p < 0.001 versus the sham group.

(F) Original images and quantification show the cellular distribution of heteromeric GluA1-GluA2 PLA signals (red) in HEK293 cells cotransfected with GluA1/GluA2 and α2δ-1-IRES-GFP or GFP (green). Scale bar, 10 μm. n = 4 per group. ***p < 0.001 versus the GFP group.

(G) Original images and quantification show the distribution of GluA1-GluA2 PLA signals (green) in the superficial dorsal horn of rats subjected to SNL or sham surgery. Thick white lines outline the lamina II region. Scale bar, 50 μm (left) and 10 μm (right). n = 4 per group. ***p < 0.001 versus the sham group.

Mann-Whitney U test was conducted in (B)–(F).
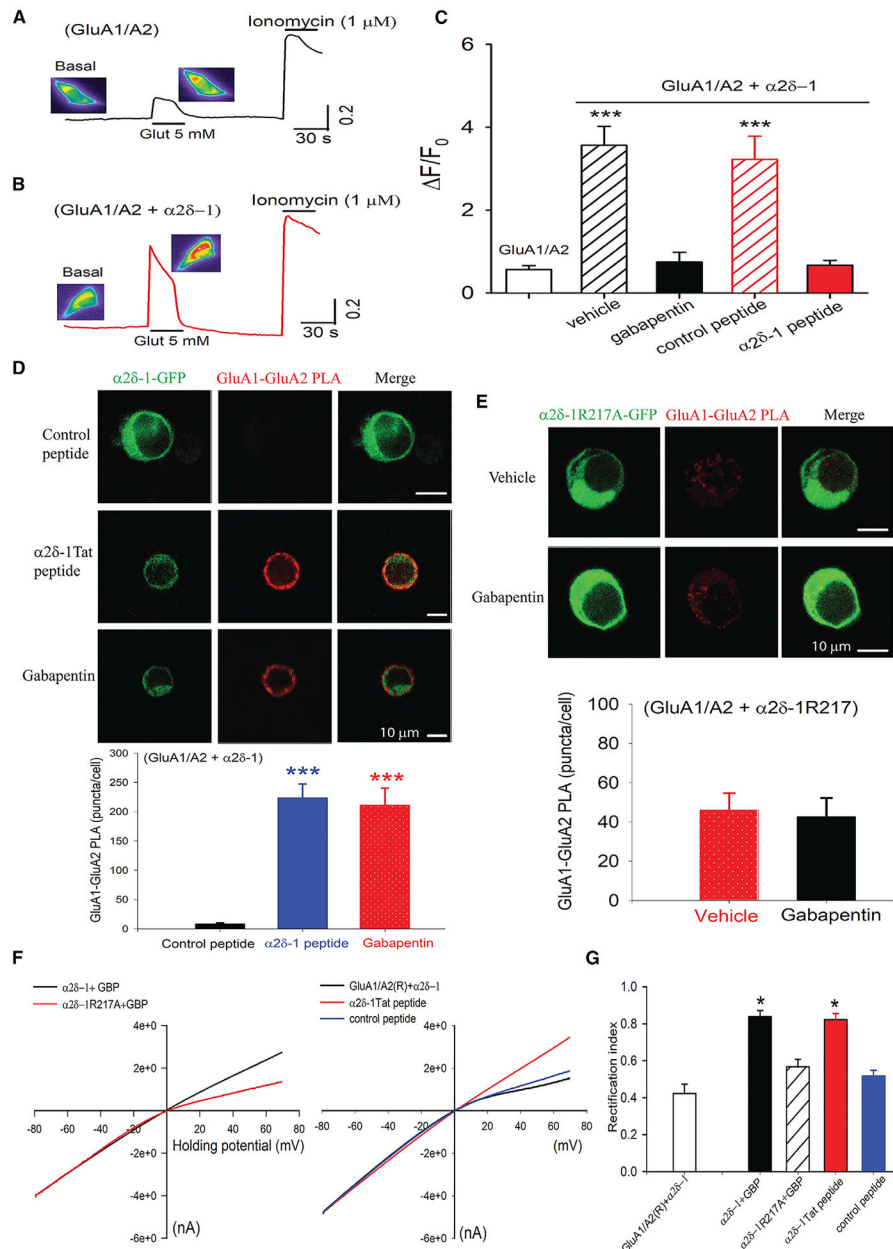
Figure 6. Gabapentin and the α2δ-1CT-Tat C terminus peptide restore heteromeric GluA1/ GluA2 receptors diminished by α2δ-1 coexpression

(A and B) Original GCaMP images and signals show intracellular Ca^{2+} changes in response to 5 mM glutamate (Glut) in HEK293 cells transfected with GluA1/GluA2 (A) or GluA1/ GluA2/α2δ-1 (B).

(C) Mean data show effects of treatment with vehicle (n = 54 cells), gabapentin (100 μM, n = 28 cells), α2δ-1CT-Tat peptide (1 μM, n = 26 cells), or control peptide (1 μM, n = 21 cells) on the ratio (F/F0) of GCaMP signals elicited by glutamate. ***p < 0.001 versus GluA1/GluA2 only (n = 56 cells). One-way ANOVA followed by Tukey test.

(D) Original PLA images and quantification show the effect of 100 μM gabapentin, 1 μM α2δ-1CT-Tat peptide, or 1 μM control peptide on heteromeric GluA1/GluA2 protein

complexes (red) in HEK293 cells cotransfected with GluA1/GluA2 and α2δ-1-IRES-GFP (green). Scale bar, 10 μm. ***$p < 0.001$ versus control peptide (n = 4 per group). Kruskal-Wallis test.

(E) Original images and quantification show the lack of an effect of gabapentin on heteromeric GluA1-GluA2 PLA signals diminished by α2δ-1R217A coexpression in HEK293 cells (n = 4 per group). Scale bar, 10 μm.

(F and G) I-V plots of glutamate-elicited currents (F) and quantification of the rectification index (G) show the effect of gabapentin (GBP), α2δ-1CT-Tat peptide, or control peptide in HEK293 cells cotransfected with GluA1/GluA2(R) and α2δ-1 or α2δ-1R217A (n = 11 cells in GluA1/A2(R)+α2δ-1, n = 12 cells in α2δ-1+GBP, n = 11 cells in α2δ-1R217A+GBP, n = 12 cells in α2δ-1CT-Tat peptide, n = 12 cells in control peptide). *$p < 0.05$ versus the untreated group (GluA1/A2(R)+α2δ-1). One-way ANOVA followed by Dunnett test.
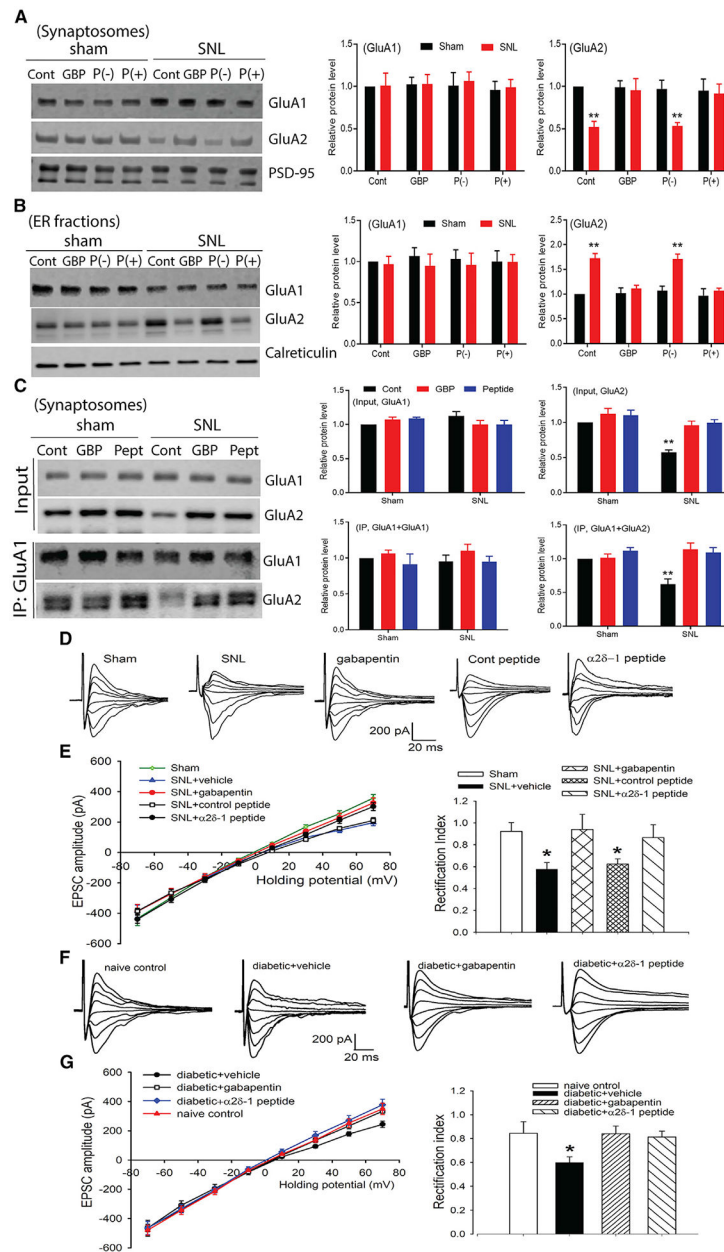
Figure 7. Gabapentin and the α2δ-1CT-Tat peptide normalize synaptic expression of GluA2-containing AMPARs in the spinal cord diminished in neuropathic pain

(A and B) Original blots and quantification show the effect of gabapentin and α2δ-1CT-Tat peptide on the protein levels of GluA1 and GluA2 in the spinal cord synaptosome (A) and the ER (B) of sham and SNL rats (n = 6 rats per group). Spinal cord slices were treated with vehicle (Cont), 100 μM GBP, 1 μM control peptide (P(−)), or 1 μM α2δ-1CT-Tat peptide (P(+)). **p < 0.01 versus the sham group. Mann-Whitney U test.

(C) Original blots and quantification show the effect of gabapentin and α2δ-1CT-Tat peptide on the protein levels of heteromeric GluA1/GluA2 protein levels in spinal cord synaptosomes of sham and SNL rats (n = 6 rats per group). **p < 0.01 versus the sham group. Kruskal-Wallis test.

(D and E) Original traces (D), I-V plots, and mean rectification index (E) of AMPAR-EPSCs of lamina II neurons in rats 3 weeks after SNL or sham surgery (n = 12 neurons). Spinal cord slices of SNL rats were treated with 100 μM gabapentin (n = 12 neurons), vehicle (n = 10 neurons), 1 μM α2δ-1CT-Tat peptide (n = 13 neurons), or 1 μM control peptide (n = 15 neurons). *p < 0.05 versus the sham group. One-way ANOVA followed by Tukey test.

(F and G) Original traces (F), I-V plots, and mean rectification index (G) of AMPAR-EPSCs of lamina II neurons in naive rats (n = 12 neurons) and diabetic rats 4 weeks after diabetic induction. Spinal cord slices were treated with 100 μM gabapentin (n = 17 neurons), vehicle (n = 14 neurons), or 1 μM α2δ-1CT-Tat peptide (n = 16 neurons). *p < 0.05 versus naive control. One-way ANOVA followed by Tukey test.

KEY RESOURCES TABLE

REAGENT or RESOURCE	SOURCE	IDENTIFIER
Antibodies		
Rabbit anti-α2δ-1	Sigma-Aldrich	C5105
Rabbit anti-α2δ-1 (extracellular)	Alomone Labs	ACC-015
Mouse anti-GluA1	NeuroMab	75-327
Rabbit anti-GluA1 (extracellular)	Alomone Labs	AGC-004
Mouse anti-GluA2	NeuroMab	75-002
Rabbit anti-GluA2 (extracellular)	Alomone Labs	AGC-005
Mouse anti-Flag	Sigma-Aldrich	F1804
Rabbit anti-Flag	Sigma-Aldrich	F7425
Mouse anti-GFP	NeuroMab	75-132
Rabbit anti-GFP	Sigma-Aldrich	G1544
Rabbit anti-Calreticulin	Cell Signaling Technology	2891
Mouse anti-PSD-95	NeuroMab	75-028
Mouse anti-alpha 1 sodium/potassium ATPase	Abcam	ab7671
Rabbit anti-GAPDH	Abcam	ab9485
Peroxidase Donkey anti-rabbit IgG	Jackson ImmunoResearch	711-035-152
Peroxidase Goat anti-mouse IgG	Jackson ImmunoResearch	115-035-003
Rabbit TrueBlot anti-rabbit IgG HRP	VWR	18-8816-33
Rabbit TrueBlot anti-mouse IgG HRP	VWR	18-8817-33
Mouse IgG	Millipore/Sigma	PP54
Rabbit IgG	Millipore/Sigma	PP64
Chemicals, peptides, and recombinant proteins		
IEM-1460	Tocris	1636
Gabapentin	Tocris	0608
Streptozotocin	Sigma-Aldrich	S0130
L-Glutamate	Sigma-Aldrich	49621
Bicuculline	Sigma-Aldrich	14343
(2R)-amino-5-phosphonopentanoate (AP5)	Abcam	ab120003
Spermine	Sigma-Aldrich	85590
Dulbecco's modified Eagle medium (DMEM)	Corning	10-013-CV
Fetal bovine serum	Sigma-Aldrich	F4135
Penicillin/Streptomycin	Corning	30-002-CI
α2δ-1 C Terminus-Tat peptide	Bio Basic Inc.	N/A
Tat-conjugated scrambled control peptide	Bio Basic Inc.	N/A
Lipofectamine 3000	Invitrogen	L3000015
Protease and phosphatase inhibitors	Thermo Fisher Scientific	78440
4-15% Mini-PROTEAN Precast Protein Gels	Bio-Rad	4560000
DC Protein Assay Kit II	Bio-Rad	5000122
Pierce Fast Western Blot Kit, ECL Substrate	Thermo Fisher Scientific	35050

REAGENT or RESOURCE	SOURCE	IDENTIFIER
Protein A/G beads	Millipore/Sigma	16-266
RIPA Lysis Buffer	Thermo Fisher Scientific	89900
IP Lysis Buffer	Thermo Fisher Scientific	87787
Pierce Cell Surface Protein Isolation Kit	Thermo Fisher Scientific	89881
GenElute HP Endotoxin-Free Plasmid Maxiprep Kit	Sigma-Aldrich	NA0410
Duolink *In Situ* Orange Starter Kit (mouse/rabbit)	Sigma-Aldrich	DUO92102
QuickChange Site-Directed Mutagenesis Kit	Agilent Technologies	200521
In-Fusion HD Cloning Plus	Clontech Laboratories	638916
Experimental models: Organisms/strains		
Cacna2d1$^{-/-}$	Medical Research Council	N/A
Sprague Dawley rats	Envigo	N/A
HEK293 cells	ATCC	CRL-1573
HEK293FT cells	Thermo Fisher Scientific	R70007
Recombinant DNA		
pcDNA3.1	Addgene	V790-20
GFP-GluA1 (C terminus)	Addgene	34857
GFP-GluA2 (C terminus)	Addgene	24003
Cacna2d2	Addgene	58732
Cacna2d3	Addgene	58727
α2δ-1-HA	Addgene	58729
α2δ-2-HA	Addgene	58733
α2δ-3-HA	Addgene	58728
Flag-α2δ-1	This paper	N/A
GFP-α2δ-1	This paper	N/A
α2δ-1R217A	Chen et al., 2018	https://doi.org/10.1016/j.celrep.2018.02.02
α2δ-1-PC	Gift from Dr. C. Eroglu	N/A
α2-PC	Gift from Dr. C. Eroglu	N/A
δ-1-PC	Gift from Dr. C. Eroglu	N/A
VWA-PC	Gift from Dr. C. Eroglu	N/A
δ-1 CT-PC	This paper	N/A
CT-PC	This paper	N/A
pLenti-α2δ-1-GFP	This paper	N/A
pLenti-GFP-α2δ-1	This paper	N/A
pLenti-α2δ-1CT	This paper	N/A
Biological samples		
Human spinal cord tissue samples	University of Maryland Brain and Tissue Bank	N/A
Software and algorithms		
Prism 8.0	GraphPad Software	https://www.graphpad.com/
ImageJ	NIH	https://imagej.nih.gov/ij/download.html
Clampfit 10.0 software	Axon Instruments	https://www.moleculardevices.com/